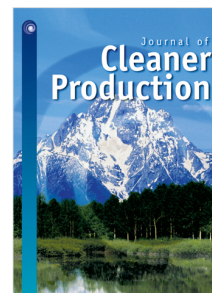


## Journal Pre-proof

Normal Boundary Intersection with factor analysis approach for multiobjective stochastic optimization of a cladding process focusing on reduction of energy consumption and rework

Simone C. Streitenberger, Estevão L. Romão, Anderson P. Paiva, Pedro P. Balestrassi, José H.G. Freitas, Vinicius C. Paes



PII: S0959-6526(21)04082-8  
DOI: <https://doi.org/10.1016/j.jclepro.2021.129915>  
Reference: JCLP 129915

To appear in: *Journal of Cleaner Production*

Received date: 19 December 2019

Revised date: 11 October 2021

Accepted date: 26 November 2021

Please cite this article as: S.C. Streitenberger, E.L. Romão, A.P. Paiva et al., Normal Boundary Intersection with factor analysis approach for multiobjective stochastic optimization of a cladding process focusing on reduction of energy consumption and rework. *Journal of Cleaner Production* (2021), doi: <https://doi.org/10.1016/j.jclepro.2021.129915>.

This is a PDF file of an article that has undergone enhancements after acceptance, such as the addition of a cover page and metadata, and formatting for readability, but it is not yet the definitive version of record. This version will undergo additional copyediting, typesetting and review before it is published in its final form, but we are providing this version to give early visibility of the article. Please note that, during the production process, errors may be discovered which could affect the content, and all legal disclaimers that apply to the journal pertain.

© 2021 Published by Elsevier Ltd.

1  
2  
3  
4  
5  
6  
7  
8  
9 Wordcount: 7157

10  
11 Highlights

- 12 • Quality and sustainability on the cladding process were investigated.
- 13
- 14 • Two-Phased Optimization (TPO) methodology was proposed.
- 15
- 16 • TPO results for quality were applied for the sustainability approach.
- 17
- 18 • The final results shown that quality can still be hold in a sustainable
- 19 process.
- 20
- 21
- 22
- 23
- 24
- 25
- 26
- 27
- 28
- 29
- 30
- 31
- 32
- 33
- 34
- 35
- 36
- 37
- 38
- 39
- 40
- 41
- 42
- 43
- 44
- 45
- 46
- 47
- 48
- 49
- 50
- 51
- 52
- 53
- 54
- 55
- 56
- 57
- 58
- 59
- 60
- 61
- 62
- 63
- 64
- 65

1  
2  
3  
4  
5  
6  
7  
8  
9  
10  
11  
12  
13  
14  
15  
16  
17  
18  
19  
20  
21  
22  
23  
24  
25  
26  
27  
28  
29  
30  
31  
32  
33  
34  
35  
36  
37  
38  
39  
40  
41  
42  
43  
44  
45  
46  
47  
48  
49  
50  
51  
52  
53  
54  
55  
56  
57  
58  
59  
60  
61  
62  
63  
64  
65

# Normal Boundary Intersection with factor analysis approach for multiobjective stochastic optimization of a cladding process focusing on reduction of energy consumption and rework

Simone C. Streitenberger\*, Estevão L. Romão, Anderson P. Paiva, Pedro P. Balestrassi, José H. G. Freitas, Vinicius C. Paes

*Industrial Engineering Institute, Federal University of Itajubá, Itajubá, MG BRAZIL*

*Simone C. Streitenberger<sup>1,\*</sup>*

---

## Abstract

Recovering, recycling and reusing are some processes whose popularity is intense nowadays due to the increasing concern about sustainability and environmental issues. These processes are composed by some input variables that can be adjusted to optimize related relevant responses. The present paper, focusing on multiobjective optimization, proposes the Two-Phased Optimization Methodology based on the use of factor analysis, the Normal Boundary Intersection method and stochastic programming. A real application is developed in a cladding process of ABNT 1020 carbon steel plate using austenitic ABNT 316L stainless steel cored wire to exemplify the approach. The first stage of the methodology focuses on optimizing the geometric characteristics of the weld bead in order to improve the quality of the final product. The achieved values for the input variables were wire feed rate = 8.96m/min, arc voltage = 29.38V, welding speed = 24.21cm/min, contact tip to the workpiece distance = 17.90mm. From the comparison of the optimized geometry from Phase 1 with the real DoE experiments geometry, the scrap and rework areas are measured through a computer graphics software. Then, in the Phase 2, which focuses on a sustainability aspect, it is solved the multiobjective stochastic problem aiming the minimization of the scrap and rework jointly with the energy consumption. In this case, the optimized values for the input variables were wire feed rate = 9.95m/min, arc voltage = 28V, welding speed = 33.51cm/min, contact tip to the workpiece distance = 25.41mm. The methodology provides consistent results when dealing with a large number of responses considering the quality of the product and the environmental issues.

*Keywords:* Normal Boundary Intersection, Response Surface Methodology, Design of

---

\*Corresponding author

*Email address:* simonecs@unifei.edu.br (Simone C. Streitenberger)

## 1. Introduction

Concerns about environmental issues have been in the spotlight, so that the overall industry started to delve into alternative techniques aiming at environmental sustainability. Stakeholders involved in all levels of the production process, from the consumers to the board members, are increasingly demanding more green and aware processes (Rusinko, 2007). Exploring and following sustainable paths can lead to improvements under both economic and environmental perspectives (Zhang and Liu, 2017).

According to (Flandinet et al., 2012), the reutilization of material using recycling techniques has been encouraged by a number of countries and industries to minimize the wastes. Remanufacturing, for example, can preserve the intrinsic value of deactivated products (Peng et al., 2019) and also eliminate stages, like material processing, significantly reducing the life cycle processes (Liu et al., 2016).

The study developed in (Liu et al., 2016) points out the laser cladding as one of the most effective techniques to the automobile components remanufacturing, reasserting the emphasis given to this area. Another strategy, the stainless steel cladding process which deposits a stainless steel layer on surfaces of carbon steel or low-alloy steels (Gomes et al., 2013), emerges as an interesting method, since its base can be a common material, usually cheaper than a piece made purely from stainless steel, that would be even for disposal. This justifies the economic and environmental interests on the technique.

Thus, remanufacturing has becoming an important activity. Shakourloo (2017) proposed a new model to optimize a remanufacturing process focusing on the profit and process costs, and applied multiobjective goal programming. The greatest advantage of this kind of work is that it contributes to operations sustainability which means utilizing the available resources without compromising the needs of future generations.

1  
2  
3  
4  
5  
6  
7  
8  
9  
10  
11  
12  
13  
14  
15  
16  
17  
18  
19  
20  
21  
22  
23  
24  
25  
26  
27  
28  
29  
30  
31  
32  
33  
34  
35  
36  
37  
38  
39  
40  
41  
42  
43  
44  
45  
46  
47  
48  
49  
50  
51  
52  
53  
54  
55  
56  
57  
58  
59  
60  
61  
62  
63  
64  
65

Aiming to combine an optimized geometry of the weld bead with the environmental issues, the Two-Phased Optimization (TPO) methodology based on factor analysis and Normal Boundary Intersection (NBI) is presented. It is exemplified through the optimization of a cladding process of ABNT 1020 carbon steel plate using austenitic ABNT 316L stainless steel cored wire, which is considered a type of recovering approach.

The present paper is structured as follow: section 2 presents the investigated related work, section 3 a background and literature review about RSM, multi-objective stochastic programming, NBI, factor analysis, and Multivariate Mean Square Error (MMSE). Section 4 presents the aforementioned case under two different perspectives: (i) process quality, optimizing the geometric characteristics of the weld bead; (ii) sustainability, through the multiobjective stochastic optimization aiming the minimization of the amount of the material involved in the rework process jointly with the cost of energy consumption. Finally in section 5, we state the conclusions of the paper.

## 2. Related Work

In the present section different papers regarding RSM published in the Journal of Cleaner Production from 2015 to 2019 are evaluated. The research was developed in the journal own basis utilizing the term "response surface methodology" as the search criterion. Only the results related to research articles were considered, discarding others like review articles and short communications. The selected works contains the exact term in their title. Table A.1 in Appendix A shows the 26 investigated articles' authors, year of publication and titles.

The following characteristics were explored: i) the convexity of the function(s); ii) the optimization direction (maximization or minimization); iii) number of factors considered; iv) number of responses; v) number of center points; vi) whether the authors developed a multiobjective optimization or not; vii) whether the authors evaluated the correlation among the considered responses or not; viii) whether the authors considered the constraint related to the exper-

1  
2  
3  
4  
5  
6  
7  
8  
9 imental region or not.

10 Among the 26 articles, we found 13 in which the objective functions are op-  
11  
12 60 timized simultaneously and 13 in which there was only one objective function or  
13 the authors did not treat the problem as a multiobjective optimization. Hence,  
14 by using the Chi-Square Goodness-of-Fit test, it leads the conclusion that both  
15 uni and multiobjective problems occur with the same frequency since a p-value  
16 equal to 0.847 was obtained.  
17  
18  
19

20 65 Another important issue investigated in the papers was the method used to  
21 solve the optimization problem. 18 papers used the Desirability algorithm to  
22 find the optimal solution. This approach does not take into account the experi-  
23 mental region constraint, what may lead to a solution outside this region, which  
24 is not reliable. Furthermore, the correlation among the responses is neglected as  
25 well. Only one paper explicitly mentioned about the correlation among the re-  
26  
27  
28 70 well. Only one paper explicitly mentioned about the correlation among the re-  
29 sponses. The remaining 8 papers did not even mention how the optimal solution  
30 was reached.  
31  
32

33 Considering the functions developed in the papers, it was analyzed if their  
34 convexity and the optimization direction were coincident. It did not happen in  
35  
36 75 66% of the cases. There were convex functions to be maximized and concave  
37 functions to be minimized, which would oblige the use of the experimental  
38 region constraint.  
39  
40  
41

### 42 **3. Background and literature review**

#### 43 *3.1. Response Surface Methodology*

44  
45  
46 80 Response Surface Methodology (RSM) is a collection of techniques used  
47 to model and to analyze problems in different contexts in which a response  
48 variable is affected by several input variables. Lu and Xu (2017) used this  
49 methodology aiming to find the best conditions to a novel strategy to recover  
50 non-leaching gold from wasted memory cards. Costa et al. (2016b) developed  
51 a multivariate optimization for a dry end milling process of AISI 1045, which  
52  
53  
54 85 a multivariate optimization for a dry end milling process of AISI 1045, which  
55 is more sustainable than conventional milling process, because it does not use  
56  
57  
58  
59  
60  
61  
62  
63  
64  
65

1  
2  
3  
4  
5  
6  
7  
8  
9 cutting fluids. Klepa et al. (2019) built up a study which aimed to obtain a  
10 raw material mixing Construction Waste (CW) with zinc oxide (ZnO) to use  
11 as a thermoluminescent sensor, performing an experiment to obtain a product  
12 with minimum ZnO content but maximum luminescence through the RSM.  
13  
14 90 with minimum ZnO content but maximum luminescence through the RSM.  
15 Nasiri and Arsalani (2018) used RSM in order to evaluate the influence of the  
16 experimental factors such as initial dye concentration, contact time, initial pH,  
17 and adsorbent dosage on the crystal violet removal efficiency and then to find  
18 optimal condition for these factors that maximizes the response function.  
19  
20

21  
22 95 Generally, the objective is to optimize the response, thus the first step in  
23 RSM is to find the mathematical model that is able to explain a relationship  
24 between the input and the output variables. It is recommended to develop  
25 a factorial design with central points which allows the approximation of this  
26 relationship to a first-order model (Montgomery, 2013) as shown in Eq. (1).  
27  
28  
29  
30

$$31 \quad y = \beta_0 + \beta_1 x_1 + \beta_2 x_2 + \dots + \beta_k x_k + \epsilon \quad (1)$$

32  
33 100 Since the main goal is to optimize the response variable, it is necessary  
34 to verify if there is a curvature in the experimental region, by calculating the  
35 difference between the average of the  $n_f$  factorial runs, i.e.,  $\bar{y}_f$ , and the average  
36 of the  $n_c$  runs in the center points, i.e.,  $\bar{y}_c$ . If this difference is small, then the  
37 center points lie on the plane passing through the factorial points or at least  
38 near this plane, otherwise it is likely to exist a curvature in the experimental  
39 region (Montgomery, 2013). The Sum of Squares for pure quadratic curvature  
40 is shown in Eq. (2)  
41  
42 105  
43  
44  
45  
46

$$47 \quad SS_{Pure\ quadratic} = \frac{n_f n_c (\bar{y}_f - \bar{y}_c)^2}{n_f + n_c} \quad (2)$$

48  
49 This sum of squares must be incorporated in the ANOVA and a hypothesis  
50 test for the curvature must be performed. Obtaining a p-value smaller than 0.05  
51 indicates that there is a curvature in that region. Otherwise, the experimenter  
52 still needs to evaluate other ranges for the factors in order to find a region  
53 where the curvature is present. The methods of steepest ascent and steepest  
54  
55  
56  
57  
58  
59  
60  
61  
62  
63  
64  
65

descent are commonly used to encounter that region and they are detailed in (Montgomery, 2013).

115 If there is curvature, a polynomial of a higher degree must be used, such as the second-order model shown in Eq. (3) (Montgomery, 2013). The performed design must be complemented with the axial points to obtain a Central Composite Design (CCD), that is extensively used for estimating second-order response surface (Costa et al., 2016b).

$$y = \beta_0 + \sum_{i=1}^k \beta_i x_i + \sum_{i=1}^k \beta_{ii} x_i^2 + \sum_{i < j} \sum_{i < j} \beta_{ij} x_i x_j + \epsilon \quad (3)$$

120 It is feasible and desirable to obtain an experimental design which insures a constant variance at all points at the same distance from the center. It can be defined as a rotatable design. Furthermore, if the design matrix ( $N \times k$ ) is chosen in a way that the matrix  $X'X$  is diagonal, the design can also be defined as an orthogonal design (Box and Hunter, 1957).

125 In order to understand how to define the radius of the axial points, and the importance of the number of center points in a CCD rotatable design, suppose we have a CCD for  $k = 2$ , whose factorial block consists of a Full Factorial Design (FFD) with levels  $= r$ . In a traditional FFD,  $r = \pm 1$ , as depicted in Fig. 1(a). Hence, it is possible to obtain the well-known mathematical expression, shown in Eq. (4), which is used to calculate the radius of a CCD with  $k$  factors, maintaining the rotatability properties of the design.

$$\rho = \sqrt[4]{2^k} \quad (4)$$

The  $\rho$  value is essential for the experimental region constraint establishment. The main advantages of this constraint, applied in scientific research (Gaudêncio et al., 2019; Pereira et al., 2017; Paiva et al., 2014; Gomes et al., 2012; Costa et al., 2016a), relies on avoiding the extrapolation, i.e., finding optimal values for the input variables outside the sphere formed by the axial points observed in Fig. 1(b).



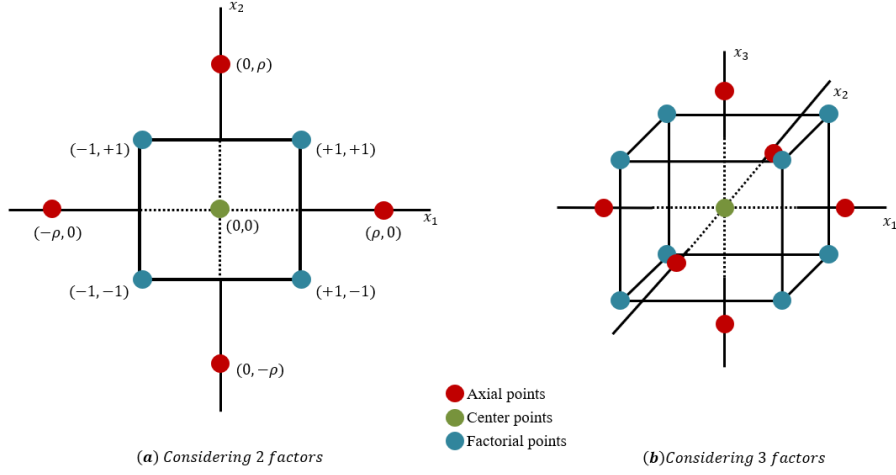


Figure 1: 2D and 3D representation for the Central Composite Design (Adapted from Montgomery (2013))

In addition, to be orthogonal, the design must have the number of center points according to Eq. (5). It is important to highlight that  $N = 2^k + n_0 + 2k$ , where  $2^k$ ,  $n_0$ , and  $2k$  represents the number of factorial points, center points, and axial points, respectively.

$$n_0 = 4\left(2^{\frac{k}{2}}\right) + 4 - 2k \quad (5)$$

### 3.2. Multiobjective Stochastic Programming

According to (Díaz-García et al., 2005), in the RSM context, we are usually interested in the optimization of a second order model, as shown in Eq. (6).

$$\begin{aligned} \min_{\mathbf{x}} \hat{Y}(\mathbf{x}, \hat{\beta}) \\ \text{s.t. } \|\mathbf{x}\|^2 = x_1^2 + \dots + x_k^2 \leq \xi^2 \end{aligned} \quad (6)$$

where  $\xi^2$  is a known constant related to the experimental space constraint.

The polynomial to be minimized was already presented in Eq. (3). How-

ever, considering the uncertainties in the calculated coefficients the deterministic model becomes the stochastic one denoted by Eq. (7).

$$\hat{Y}(\mathbf{x}, \hat{\beta}) = \hat{\beta}_0 + \sum_{i=1}^k \hat{\beta}_i x_i + \sum_{i=1}^k \hat{\beta}_{ii} x_i^2 + \sum_{i<j}^k \hat{\beta}_{ij} x_i x_j \equiv z'(\mathbf{x}) \hat{\beta} \quad (7)$$

where  $z(\mathbf{x})$  is a vector that contains the polynomial terms of the  $k$  predictors in  $\mathbf{x}$  and  $\hat{\beta}$  is the vector of least squares regression coefficients. These coefficients are not deterministic, since we are considering  $Y_i = z'(\mathbf{x}_i) \beta + \epsilon_i$ , with  $\epsilon_i \sim N(0, \sigma^2)$ ,  $\epsilon_i$ 's independent for  $i = 1, \dots, n$ , and  $\hat{\beta} \sim N_p(\beta, \sigma^2(X'X)^{-1})$ , with  $p = 1 + k + k(k+1)/2$  and  $(n-p)\hat{\sigma}^2/\sigma^2 \sim \chi_{n-p}^2$ , being  $\hat{\sigma}^2$  the unbiased estimator of  $\sigma^2$  and  $X$  is the  $n \times p$  design matrix of rank  $p$  (Díaz-García et al., 2005).

Hence, in a stochastic problem, the response variables, the controllable variables and even some parameters involved may have a random character (Díaz-García and Bshiri, 2014). Some problems with multiple responses and that consider the presence of uncertainties can be viewed in (Yang et al., 2018) (Fu et al., 2019) (Shabani and Sowlati, 2016) (Ren et al., 2019).

A very useful approach related to the stochastic programming is the dual problem in which the functions being optimized are the mean and the variance of a response variable. Thus, considering the presence of uncertainties in the objective function and in the constraints, it is possible to model a problem in which the objective is to minimize the value of the mean plus the variance of a response variable subjected to the value of the the mean plus the standard deviation of a second response variable as shown in Eq. (8).

$$\begin{aligned} \min_x F(x) &= w_1(\mathbf{x}^T \beta) + (1 - w_1)[\mathbf{x}^T (\tilde{\Sigma}_\beta) \mathbf{x}] \\ s.t. \quad g_1(\mathbf{x}) &= \mathbf{x}^T \gamma + s_i \sqrt{\mathbf{x}^T (\tilde{\Sigma}_\beta) \mathbf{x}} - c \leq 0 \\ g_2(\mathbf{x}) &= \mathbf{x}^T \mathbf{x} \leq \xi^2 \end{aligned} \quad (8)$$

where  $w_1$  represents the weight associated to the first portion of the objective function,  $\mathbf{x}^T \beta$  and  $\mathbf{x}^T (\tilde{\Sigma}_\beta) \mathbf{x}$  represent the mean and the variance of the first

1  
2  
3  
4  
5  
6  
7  
8  
9  
10 response variable, respectively.  $\mathbf{x}^T\boldsymbol{\gamma}$  and  $\sqrt{\mathbf{x}^T(\hat{\boldsymbol{\Sigma}}_{\beta})\mathbf{x}}$  indicate the mean and the  
11 standard deviation of the second response variable. The value of  $s_i$  is the z-score  
12 related to the probability of the constraint  $g_1(\mathbf{x})$  to be satisfied, whereas  $c$  is a  
13 constant defined by the researcher.  
14

### 15 3.3. Normal Boundary Intersection

16  
17  
18 Since most of real cases involves the optimization of two or more functions  
19 with conflicting objectives, it requires more sophisticated strategies to obtain  
20 satisfactory results. Das and Dennis (1998) proposed a method called Nor-  
21 mal Boundary Intersection (NBI) which provides different equidistant optimal  
22 solutions that together form the Pareto's Frontier.  
23

24  
25 According to (Brito et al., 2014), for a bi-objective case, the problem can be  
26 expressed in terms of Eq. (9).  
27  
28

$$\begin{aligned}
 & \min \bar{f}_1(x) \\
 & \text{s.t. : } \bar{f}_1(x) - \bar{f}_2(x) + 2w - 1 = 0 \\
 & \quad g_j(x) \geq 0 \\
 & \quad 0 \leq w \leq 1
 \end{aligned} \tag{9}$$

29  
30  
31 where  $\bar{f}_1(x)$  and  $\bar{f}_2(x)$  are the objective functions normalized according to  
32 Eq. (10).  
33  
34

$$\bar{f}(x) = \frac{f_i(x) - f_i^U}{f_i^N - f_i^U} \tag{10}$$

35  
36 The Utopia and Nadir values,  $f_i^U$  and  $f_i^N$  respectively, represent the best  
37 and the worst values for the function being normalized. They are obtained  
38 from the Pay-Off matrix, which is composed of the individual optimum of each  
39 function on the main diagonal represented by  $f_i^*(x_i^*)$ . These optimal values of  
40 the vector  $\mathbf{x}$  must be applied in the remaining objective functions  $f_i(x_i^*)$  in order  
41  
42  
43  
44  
45  
46  
47  
48  
49  
50  
51  
52  
53  
54  
55  
56  
57  
58  
59  
60  
61  
62  
63  
64  
65

to complete a row of the Pay-Off matrix, as shown in Eq. (11).

$$\bar{\Phi} = \begin{bmatrix} f_1^*(x_1^*) & \dots & f_1(x_i^*) & \dots & f_1(x_m^*) \\ \vdots & \ddots & & & \vdots \\ f_i(x_1^*) & \dots & f_i^*(x_i^*) & \dots & f_i(x_m^*) \\ \vdots & & & \ddots & \vdots \\ f_m(x_1^*) & \dots & f_m(x_i^*) & \dots & f_m^*(x_m^*) \end{bmatrix} \quad (11)$$

Similarly, in situations whose purpose is the optimization of three or more functions simultaneously, the problem can be generically modelled following the Eq. (12).

$$\begin{aligned} & \max_{(\mathbf{x}, t)} \mathbf{D} \\ & s.t. : \bar{\Phi} \mathbf{W}_i + D \hat{\mathbf{n}} = \bar{\mathbf{F}}(\mathbf{x}) \\ & \quad \mathbf{x} \in \Omega \\ & \quad h_j(\mathbf{x}) = 0 \\ & \quad g_j(\mathbf{x}) \leq 0 \end{aligned} \quad (12)$$

where  $\bar{\Phi}$  represents the normalized Pay-Off matrix,  $\bar{\mathbf{F}}(\mathbf{x})$  is the vector of normalized objective functions,  $\mathbf{W}_i$  is the  $i$ -th vector of weights, and  $\hat{\mathbf{n}}$  is a unitary normalized vector.

Nevertheless, if the objective functions are correlated, it can cause model's instability, overfitting, and not representative regression coefficients (Wu, 2004) (Yuan et al., 2008) (Box et al., 1973). In this condition, the NBI method will probably produce unreal results (Costa et al., 2016b). Therefore, it is important to apply multivariate techniques, such as factor analysis, to cope with this (Luz et al., 2021).

#### 3.4. Factor Analysis

The essential purpose of factor analysis is to describe the covariance relationships among the response variables in terms of a few factors. An observable random vector  $\mathbf{X}$  with  $p$  components, mean  $\mu$ , and covariance matrix  $\Sigma$  is

1  
2  
3  
4  
5  
6  
7  
8  
9 linearly dependent upon a few unobservable random variables  $F_1, F_2, \dots, F_m$ ,  
10 which are called common factors, and the additional sources of variation called  
11 specific factors  $\epsilon_1, \epsilon_2, \dots, \epsilon_p$ . Then, the orthogonal factor model in matrix nota-  
12 tion is shown in Eq. (13), where  $\mathbf{L}$  represent the matrix of factor loadings with  
13 dimension  $(p \times m)$  (Johnson and Wichern, 2007).  
14  
15  
16  
17  
18  
19  
20  
21  
22

$$\mathbf{X} - \mu = \mathbf{L}\mathbf{F} + \epsilon \quad (13)$$

23  
24  
25  
26  
27  
28  
29  
30  
31  
32  
33  
34  
35  
36  
37  
38  
39  
40  
41  
42  
43  
44  
45  
46  
47  
48  
49  
50  
51  
52  
53  
54  
55  
56  
57  
58  
59  
60  
61  
62  
63  
64  
65

In order to perform the factor analysis some assumptions must be considered as shown in Eq. (14).

$$\begin{aligned} \mathbf{E}(\mathbf{F}) &= \mathbf{0}, \quad \mathbf{Cov}(\mathbf{F}) = \mathbf{E}[\mathbf{F}\mathbf{F}'] = \mathbf{I} \\ \mathbf{E}(\epsilon) &= \mathbf{0}, \quad \mathbf{Cov}(\epsilon) = \mathbf{E}[\epsilon\epsilon'] = \Psi \end{aligned} \quad (14)$$

Thus, it is possible to demonstrate that the covariance matrix can also be expressed by the Eq. (15) using the orthogonal factor model ( $X = \mu + LF + \epsilon$ ), and considering the assumptions above.

$$\begin{aligned} \Sigma = \mathbf{Cov}(\mathbf{X}) &= \mathbf{E}(\mathbf{X} - \mu)(\mathbf{X} - \mu)' \\ &= \mathbf{L}\mathbf{E}(\mathbf{F}\mathbf{F}')\mathbf{L}' + \mathbf{E}(\epsilon\mathbf{F}')\mathbf{L}' + \mathbf{L}\mathbf{E}(\mathbf{F}\epsilon') + \mathbf{E}(\epsilon\epsilon') \\ &= \mathbf{L}\mathbf{L}' + \Psi \end{aligned} \quad (15)$$

Choosing  $m$  factors,  $m \leq p$ , to represent the dataset we obtain an estimate of the covariance matrix ( $S$ ) as shown in Eq. (16).

$$\mathbf{S} = \tilde{\mathbf{L}}\tilde{\mathbf{L}}' + \tilde{\Psi}$$

$$\mathbf{S} = \begin{bmatrix} \sqrt{\hat{\lambda}_1}\hat{\mathbf{e}}_1 & \sqrt{\hat{\lambda}_2}\hat{\mathbf{e}}_2 & \dots & \sqrt{\hat{\lambda}_m}\hat{\mathbf{e}}_m \end{bmatrix} \begin{bmatrix} \sqrt{\hat{\lambda}_1}\hat{\mathbf{e}}_1' \\ \sqrt{\hat{\lambda}_2}\hat{\mathbf{e}}_2' \\ \vdots \\ \sqrt{\hat{\lambda}_m}\hat{\mathbf{e}}_m' \end{bmatrix} + \begin{bmatrix} \tilde{\psi}_1 & 0 & \dots & 0 \\ 0 & \tilde{\psi}_2 & & 0 \\ \vdots & \vdots & \ddots & \vdots \\ 0 & 0 & \dots & \tilde{\psi}_m \end{bmatrix} \quad (16)$$

In cases in which the units of the variables are not commensurate, it is convenient to work with normalized variables. Therefore, it is possible to use the estimated correlation matrix ( $R$ ) instead of the covariance matrix  $\Sigma$ .

Nevertheless, the researcher can also face some situations in which a factor contains responses with different objectives (minimization and maximization). In these situations, instead of optimizing the factors' means, we opt to minimize the value of the multivariate mean square error, explained in the next section.

### 3.5. Multivariate Mean Square Error

To overcome the problem of conflicting responses objectives represented by a same factor, Paiva et al. (2009) proposed an index called Multivariate Mean Square Error (MMSE) able to aggregate several responses, keeping their variance-covariance structure and the individual deviation from each target. The authors used Principal Components Analysis (PCA) to obtain the value of MMSE.

This approach can also be modified by using factor analysis which is considered as an extension of PCA (Leite, 2019), since both methods approximate the covariance model, although the approximation based on factor analysis is more elaborated (Johnson and Wichern, 2007). Equation (17) demonstrates how to calculate the MMSE index.

$$MMSE_j = (\mu_j - T_j)^2 \quad (17)$$

where  $\mu_j$  is the mean obtained from the optimization and  $T_j$  is the  $j$ th factor's target which can be achieved from Eq. (18).

$$T_j = \mathbf{L}_j \left( \frac{\mu_i - T_i}{\sigma_i} \right) \quad (18)$$

$\mu_i$ ,  $T_i$ , and  $\sigma_i$  represent, respectively, the individual values of mean, target, and standard deviation of each original response variable.  $L$ , represented by the  $j$ th line of the matrix  $\tilde{\mathbf{L}}\tilde{\mathbf{L}}'$ , is the vector consisting of the loadings of the factor whose target we aim to achieve, as shown in Eq. (16).

#### 4. Methodology

The methods presented in the previously section can be combined in order to obtain more accurate results in an optimization problem. Considering a manufacturing process, the main objective is to optimize the quality characteristics of the product to reach the clients' expectations. For that, we may start running a full factorial design with center points. Then, it is necessary to evaluate whether there is curvature in the analyzed region. In case of a negative response, some other experiments must be performed until an adequate region is found. Finally, we must add the axial points, so that it is viable to model functions for the output variables.

Aiming to neutralize the correlation effect among the responses, it is recommended to perform a factor analysis to work with non-correlated factors. It is up to the researcher the definition of how many factors it is interesting to work with. These factors must be modelled as polynomial functions (normally a second order polynomial tends to be satisfactory). Since the functions gathered in the factors may present conflicting optimization directions (minimization and maximization) it is convenient to consider the MMSE as the objective function to be minimized.

Thus, the NBI method can be applied for the first time to find the set of optimal solutions that minimizes the MMSE. Related to each solution there is a value of Mahalanobis' distance indicating the dispersion of the data regarding the optimum, and a value of entropy associated to the weights array used in the NBI. In this case, a mixture design can be applied to determine this weights array  $\mathbf{W}'_i = [w_1, w_2, \dots, w_j]$ , where  $i$  ranges from 1 to the number of runs in the mixture design,  $j$  is related to the numbers of defined MMSE function and the sum of  $w_1, w_2, \dots, w_j$  must total to 1. The number of runs may vary depending on the degree of lattice and the number of components, since a simplex lattice design is being considered. From Eq. (12), it is possible to state that  $i$  determines the number of NBI sub-problems and  $w_j$  the importance associated to each MMSE function.

It is possible to model the ratio entropy by Mahalanobis' distance as a function of the weights  $\mathbf{W}' = [W_1|W_2|\dots|W_i]$  used in the NBI. Considering this evaluation criterion as the objective function, we optimize the problem, aiming to maximize it. Hence, the set of weights associated to the optimum value is identified and applied on the NBI to find the best solution for the original responses.

Figure 2 shows a synthesis of the first stage of TPO methodology proposed in this paper. It is important to highlight that the actions from 1.1 up to 1.3 were already performed in (Gomes et al., 2013).

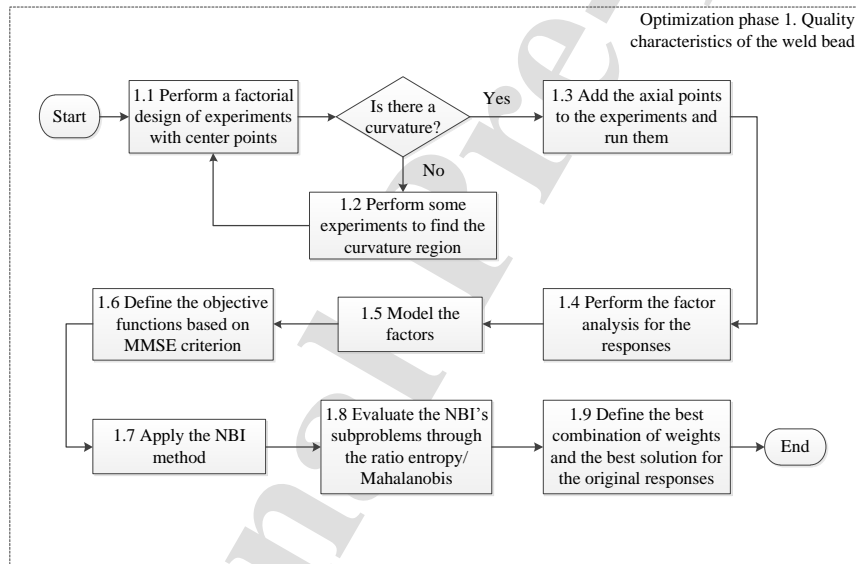


Figure 2: TPO Methodology - Phase 1

Nevertheless, applying the optimized parameters obtained in the previous step may be not sustainable regarding relevant variables, e.g., energy consumption and material involved in the rework process, which can be hazardous to the environment. Following the proposed approach in this paper, the next goal is to optimize these specific variables using a multiobjective stochastic programming. The second phase of TPO is summarized in Fig. 3.



It is worth mentioning that if the process manager needs to calculate economic indicators, such as Net Present Value (NPV), the process uncertainties will spread to the costs and reach the values of this metric, resulting in a stochastic NPV that must be optimized. Some simulation analysis focusing on the risk of failure may be developed, and then we can calculate the probability of NPV being less than 0.

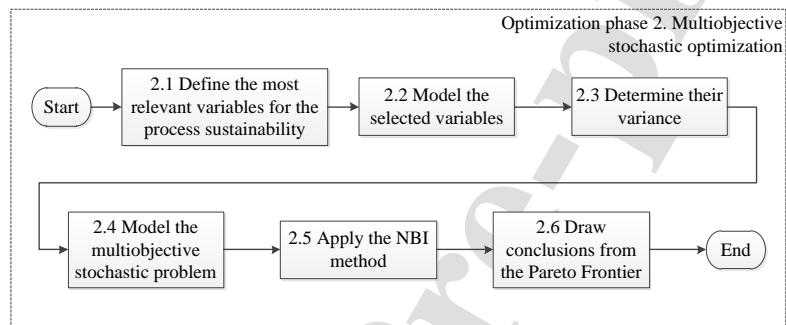


Figure 3: TPO Methodology - Phase 2

## 5. Application of TPO methodology for cladding process optimization

### 5.1. Optimization of the cladding process focusing on the geometric characteristics of the weld bead

The stainless steel cladding process has been highlighted in the industrial environment since it allows to obtain surfaces with desirable characteristics from low cost materials. This case explores the cladding of ABNT 1020 carbon steel plate using austenitic ABNT 316L stainless steel cored wire.

The equipment used for the experimentation is depicted in Fig. 4, where: (1) welding torch, (2) specimen, (3) device for the torch conduction, (4) ESAB AristoPower 460, (5) AristoFeed 30-4W MA6, (6) shielding gas cylinder, and (7) shielding gas flow meter. This equipment is available at a laboratory of Federal University of Itajubá. The considered base metal (ABNT 1020 carbon steel)

was cut into 120 x 60 x 6,35 mm plates, whereas the filler metal was a stainless steel tubular wire (AWS E316LT1-1/4) with 1,2 mm diameter.



Figure 4: Equipment used for the experimentation (Adapted from Gomes (2013))

The factors that influence the process are wire feed rate (WFR), arc voltage (AV), welding speed (WS), and contact tip to the workpiece distance (CTWD) as analyzed in (Gomes et al., 2013). The experimental levels for each one of them are depicted in Table 1.

Table 1: Parameters considered in the cladding process and their respective experimental levels

Parameters	Unit	Experimental Levels				
		-2	-1	0	1	2
Wire Feed Rate	m/min	5.5	7.0	8.5	10.0	11.5
Arc Voltage	V	24.5	27.0	29.5	32.0	34.5
Welding Speed	cm/min	20.0	30.0	40.0	50.0	60.0
Contact Tip to the Workpiece Distance	mm	10.0	15.0	20.0	25.0	30.0

After defining those factors and their respective experimental levels, it was

1  
2  
3  
4  
5  
6  
7  
8  
9  
10  
11  
12  
13  
14  
15  
16  
17  
18  
19  
20  
21  
22  
23  
24  
25  
26  
27  
28  
29  
30  
31  
32  
33  
34  
35  
36  
37  
38  
39  
40  
41  
42  
43  
44  
45  
46  
47  
48  
49  
50  
51  
52  
53  
54  
55  
56  
57  
58  
59  
60  
61  
62  
63  
64  
65

performed a factorial design with 16 cube points and 7 center points. Since the  
315 region presented curvature it were performed 8 additional experiments repre-  
sents the axial points. Figure 5 shows the weld bead from the 19<sup>th</sup> experiment  
with its respective dimensions. The 31 resulting experiments following a Central  
Composite Design were performed in (Gomes et al., 2013) and can be viewed  
in Table 2. The 10 original variables measured were: Heat Input (HI), Pene-  
320 tration (P), Penetration Area (PA), Dilution (D), Width (W), Reinforcement  
(R), Convexity Index (CI), Reinforcement Area (RA), Penetration Size Factor  
(PSF), and Reinforcement Form Factor (RFF).

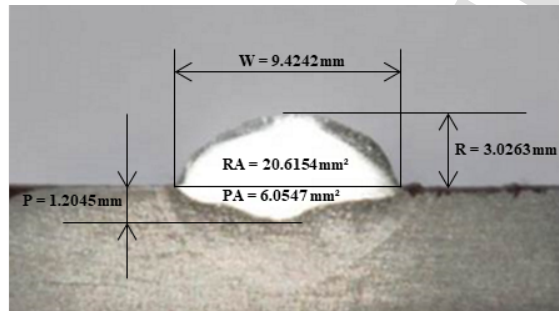


Figure 5: 19<sup>th</sup> experiment with its respective dimensions

Table 2: Experimental design and the results for 10 original variables

#	WFR	AV	WS	CTWD	HI	P	PA	D	W	R	CI	RA	PSF	RFF
1	7	27	30	15	0.9288	1.3748	7.6151	0.2644	11.1868	2.6278	0.2349	21.1787	8.1370	4.2571
2	10	27	30	15	1.1556	1.6609	9.9409	0.2582	12.9908	3.1158	0.2398	28.5077	7.8217	4.1694
3	7	32	30	15	1.1584	1.6891	9.9385	0.3149	12.6984	2.4963	0.1966	21.7027	7.5181	5.0868
4	10	32	30	15	1.4912	1.9768	14.4123	0.3125	15.0473	2.7782	0.1846	31.7181	7.6119	5.4162
5	7	27	50	15	0.5605	1.6468	7.4284	0.3622	9.2145	2.1651	0.2350	13.0586	5.5953	4.2560
6	10	27	50	15	0.6642	1.9361	9.4187	0.3369	9.9609	2.6666	0.2677	18.5681	5.1448	3.7354
7	7	32	50	15	0.6758	1.5379	7.8384	0.3712	9.7479	2.0649	0.2118	13.2965	6.3385	4.7209
8	10	32	50	15	0.8371	2.1808	12.9967	0.4108	11.5112	2.4249	0.2107	18.5934	5.2785	4.7471
9	7	27	30	25	0.7722	1.2504	6.1545	0.2246	10.3249	2.8700	0.2780	21.3626	8.2571	3.5975
10	10	27	30	25	0.9666	0.9993	6.7827	0.1832	11.4275	3.5940	0.3145	30.1513	11.4358	3.1796
11	7	32	30	25	0.9728	1.3215	6.9475	0.2371	11.2668	2.8479	0.2528	22.3884	8.5258	3.9562
12	10	32	30	25	1.1456	1.1005	8.7151	0.2196	13.3366	3.1793	0.2384	31.2054	12.1188	4.1949
13	7	27	50	25	0.4633	1.1114	4.5968	0.2496	7.9917	2.5543	0.3196	13.8134	7.1905	3.1288
14	10	27	50	25	0.5735	1.2254	5.3702	0.2331	8.6246	2.7967	0.3243	17.5415	7.0382	3.0839
15	7	32	50	25	0.5798	1.3697	5.3312	0.2877	8.4756	2.3628	0.2788	13.2206	6.1881	3.5871

Table 2: Experimental design and the results for 10 original variables

#	WFR	AV	WS	CTWD	HI	P	PA	D	W	R	CI	RA	PSF	RFF
16	10	32	50	25	0.7027	1.6370	8.0318	0.3019	10.8395	2.5983	0.2397	18.5772	6.6217	4.1718
17	5.5	29.5	40	20	0.6239	1.3822	5.8740	0.3156	9.0674	2.2068	0.2434	12.7864	6.5601	4.1089
18	11.5	29.5	40	20	0.9425	2.1393	11.5009	0.3095	12.2124	3.0557	0.2502	25.8603	5.7086	3.9966
19	8.5	24.5	40	20	0.6431	1.2045	6.0547	0.2284	9.4242	3.0263	0.3211	20.6154	7.8240	3.1142
20	8.5	34.5	40	20	0.9729	1.8644	10.2706	0.3558	11.6894	2.4578	0.2103	18.5753	6.2697	4.7560
21	8.5	29.5	20	20	1.6550	0.9476	8.5576	0.1858	14.9336	3.4536	0.2313	37.6380	15.7600	4.3241
22	8.5	29.5	60	20	0.5074	1.4328	6.6701	0.3578	8.4822	2.2498	0.2652	11.9547	5.9200	3.7702
23	8.5	29.5	40	10	0.9868	2.1784	13.2992	0.4044	11.7331	2.6103	0.2225	19.5471	5.3860	4.4949
24	8.5	29.5	40	30	0.6726	1.2825	5.8191	0.2416	9.2208	2.8912	0.3136	18.2157	7.1899	3.1892
25	8.5	29.5	40	20	0.7965	1.7082	8.3989	0.3105	10.8230	2.5960	0.2399	18.6733	6.3360	4.1691
26	8.5	29.5	40	20	0.8009	1.7229	8.7354	0.3167	10.9258	2.5923	0.2373	18.9206	6.3414	4.2147
27	8.5	29.5	40	20	0.7921	1.6230	8.4818	0.3088	10.7436	2.6549	0.2471	18.9703	6.6196	4.0466
28	8.5	29.5	40	20	0.7788	1.8014	8.7737	0.3283	10.6118	2.4950	0.2351	17.9509	5.8908	4.2532
29	8.5	29.5	40	20	0.7744	1.4854	7.8761	0.2999	10.6355	2.6208	0.2464	18.4664	7.1602	4.0581
30	8.5	29.5	40	20	0.7611	1.4897	8.2041	0.3109	10.5862	2.6119	0.2467	18.2076	7.1062	4.0531

Table 2: Experimental design and the results for 10 original variables

#	WFR	AV	WS	CTWD	HI	P	PA	D	W	R	CI	RA	PSF	RFF
31	8.5	29.5	40	20	0.7700	1.5041	8.0139	0.3102	10.5711	2.5574	0.2419	17.8624	7.0281	4.1335

1  
2  
3  
4  
5  
6  
7  
8  
9  
10  
11  
12  
13  
14  
15  
16  
17  
18  
19  
20  
21  
22  
23  
24  
25  
26  
27  
28  
29  
30  
31  
32  
33  
34  
35  
36  
37  
38  
39  
40  
41  
42  
43  
44  
45  
46  
47  
48  
49  
50  
51  
52  
53  
54  
55  
56  
57  
58  
59  
60  
61  
62  
63  
64  
65

It is important to mention that the experiments from 1 to 16 represent the full factorial design and it is also possible to observe, as previously mentioned in Eq. (4), that the value of  $\rho = \sqrt[4]{2^4}$ , is applied to generate the axial points, represented by the 17<sup>th</sup> to 24<sup>th</sup> experiments.

However, the axial points were added after the analysis of the center points, represented by the experiments from 25 to 31, in order to verify the presence of curvature. The analysis of variance for the response variable HI is shown in Table 3, where A, B, C, and D indicate WFR, AV, WS, and CTWD, respectively. It is highlighted in bold the p-value related to the curvature, 0.000, which indicates a high probability of existing a curvature in the analyzed region, and the value of the Sum of squares for pure quadratic curvature, which is calculated as previously shown in Eq. (2).

The same analysis was performed for the other variables and the related p-values can be observed in Table 4.

Analyzing the DOE it is possible to obtain the mathematical models for each response, the values of  $R_{adj}^2$  and the values of Adjusted Mean Square for the Error source which are shown in equations from Eq. (19) to Eq. (28). In addition, all the residuals were evaluated as normally distributed.

$$\begin{aligned}
 HI &= 0.788 + 0.086x_1 + 0.089x_2 - 0.243x_3 - 0.080x_4 + 0.070x_3^2 - 0.027x_1x_3 \\
 &\quad - 0.026x_2x_3 + 0.029x_3x_4 \\
 R_{adj}^2 &= 99.60\% \\
 AdjMSE &= 0.0020 \\
 S &= 0.0047
 \end{aligned}
 \tag{19}$$

Table 3: Analysis of variance for the response variable HI

Source	DF	Adj SS	Adj MS	F-Value	P-Value
Model	14	1.221	0.087	396.490	0.000
Linear	4	1.149	0.287	1305.460	0.000
WFR	1	0.127	0.127	576.610	0.000
AV	1	0.137	0.137	621.140	0.000
WS	1	0.781	0.781	3547.680	0.000
CTWD	1	0.105	0.105	476.420	0.000
2-Way Interactions	6	0.043	0.007	32.62	0.000
A*B	1	0.002	0.001	6.800	0.031
A*C	1	0.011	0.011	52.230	0.000
A*D	1	0.003	0.003	14.290	0.005
B*C	1	0.011	0.011	47.930	0.000
B*D	1	0.003	0.003	14.780	0.005
C*D	1	0.013	0.013	59.710	0.000
3-Way Interactions	3	0.005	0.002	7.190	0.012
A*B*D	1	0.002	0.002	8.45	0.020
A*C*D	1	0.002	0.002	7.31	0.027
B*C*D	1	0.001	0.001	5.82	0.042
Curvature	1	<b>0.025</b>	0.025	111.730	<b>0.000</b>
Error	8	0.002	0.000		
Lack-of-Fit	2	0.000	0.000	1.000	0.422
Pure Error	6	0.001	0.000		
Total	22	1.223			

Table 4: P-values for the curvature analysis of the indicated response variables

	HI	P	PA	D	W	R	CI	RA	PSF	RFF
SS	0.025	0.068	0.089	0.003	0.227	0.055	0.000	30.297	4.042	0.013
p-value	0.000	0.049	0.420	0.000	0.007	0.001	0.002	0.000	0.001	0.159



$$\begin{aligned}
P &= 1.632 + 0.122x_1 + 0.122x_2 + 0.093x_3 - 0.241x_4 - 0.117x_3^2 + 0.076x_1x_3 \\
&\quad - 0.100x_1x_4 \\
R_{adj}^2 &= 84.08\% \\
AdjMSE &= 0.0166 \\
S &= 0.129
\end{aligned} \tag{20}$$

$$\begin{aligned}
PA &= 8.299 + 1.295x_1 + 1.056x_2 - 0.553x_3 - 1.776x_4 - 0.227x_3^2 + 0.259x_4^2 \\
&\quad + 0.524x_1x_2 - 0.505x_1x_4 - 0.291x_2x_4 \\
R_{adj}^2 &= 97.49\% \\
AdjMSE &= 0.1711 \\
S &= 0.414
\end{aligned} \tag{21}$$

$$\begin{aligned}
D &= 0.310 - 0.003x_1 + 0.025x_2 + 0.037x_3 - 0.043x_4 - 0.007x_2^2 \\
&\quad - 0.012x_3^2 + 0.008x_1x_2 - 0.008x_3x_4 \\
R_{adj}^2 &= 97.23\% \\
AdjMSE &= 0.0002 \\
S &= 0.015
\end{aligned} \tag{22}$$

$$\begin{aligned}
W &= 10.640 + 0.797x_1 + 0.656x_2 - 1.451x_3 - 0.629x_4 + 0.270x_3^2 + 0.266x_1x_2 \\
R_{adj}^2 &= 99.37\% \\
AdjMSE &= 0.0626 \\
S &= 0.250
\end{aligned} \tag{23}$$

$$R = 2.592 + 0.203x_1 - 0.116x_2 - 0.262x_3 + 0.126x_4 + 0.030x_2^2 + 0.057x_3^2 + 0.032x_4^2 - 0.047x_1x_2$$

$$R_{adj}^2 = 97.82\% \quad (24)$$

$$AdjMSE = 0.0103$$

$$S = 0.102$$

$$CI = 0.243 + 0.001x_1 - 0.026x_2 + 0.009x_3 + 0.027x_4 + 0.005x_2^2 + 0.005x_4^2 - 0.009x_1x_2$$

$$R_{adj}^2 = 98.18\%$$

$$AdjMSE = 0.0001$$

$$S = 0.009$$

(25)

$$RA = 19.079 + 3.375x_1 - 5.538x_3 + 1.570x_3^2 - 0.941x_1x_3$$

$$R_{adj}^2 = 99.33\%$$

$$AdjMSE = 1.0450$$

$$S = 1.023$$

(26)

$$PSF = 6.534 + 0.151x_1 - 1.738x_3 + 0.731x_4 + 1.057x_3^2 - 0.486x_1x_3 + 0.549x_1x_4$$

$$R_{adj}^2 = 94.22\%$$

$$AdjMSE = 0.7003$$

$$S = 0.837$$

(27)

$$\begin{aligned}
RFF &= 4.103 - 0.005x_1 + 0.407x_2 - 0.147x_3 - 0.421x_4 - 0.051x_4^2 + 0.141x_1x_2 \\
R_{adj}^2 &= 98.03\% \\
AdjMSE &= 0.0232 \\
S &= 0.153
\end{aligned}
\tag{28}$$

In order to evaluate if these functions are concave or convex it is necessary to calculate the gradient and the hessian of the functions. The next step is to calculate the eigenvalues of the hessian matrix. If they are both positive the function is strictly convex or both negative the function is strictly concave. There is also the possibility of eigenvalues equal to zero, in this case the set of eigenvalues may be non-negative or non-positive and the function will be classified only as convex or concave, respectively. Another important point is that the hessian matrix may present a set of eigenvalues consisting on positive and negative values, characterizing a saddle point.

Basically, an optimum process in terms of quality is the one which covers the maximum surface of the base material, maximizes the reinforcement, and produces a sufficient penetration. However, a very large reinforcement may represent rework, because after cladding we generally need to improve the surface quality through machining. To cope with it, the multiobjective approach do not allow the reinforcement to be maximized indiscriminately, since the other response variables also dispute to reach their optimum values.

In this cladding process, it is not necessary a large penetration, since the main objective is to obtain a surface which only incorporates the characteristics of the material being added. Regarding the environmental and economic perspectives, the process can reach its optimum scenario through the minimization of the Heat Input (HI), that will lead to a minimum energy cost. Table 5 shows all the original variables, their respective optimization directions, their convexity and a column indicating if the convexity and the optimization direction are coincident. It is important to highlight that the Convexity Index

365 (R/W), Penetration Size Factor (W/P), and Reinforcement Form Factor (W/R)  
 are dimensionless, and the Dilution  $[PA/(PA+RA)]$  is a percentage value.

Table 5: Original variables and their respective optimization directions

Response variables	Unit	Optimization direction	Convexity	Conflicting
Heat Input	J/cm	Minimization	Saddle	Yes
Penetration	mm	Minimization	Saddle	Yes
Penetration Area	$mm^2$	Minimization	Saddle	Yes
Dilution	%	Minimization	Saddle	Yes
Width	mm	Maximization	Saddle	Yes
Reinforcement	mm	Maximization	Saddle	Yes
Convexity index	-	Minimization	Saddle	Yes
Reinforcement Area	$mm^2$	Maximization	Saddle	Yes
Penetration Size Factor	-	Maximization	Saddle	Yes
Reinforcement Form Factor	-	Maximization	Saddle	Yes

As mentioned in the section 2, once all the functions present saddle points, it is possible to understand how important is the experimental region constraint in the optimization problem. The value of  $\rho$  will be used afterwards since  $\mathbf{X}'\mathbf{X}$  must be less than  $\sqrt{2^k} = \rho^2 = 2^2$ . Hence, when optimizing each response, the constraint will be active, since the optimization direction and the convexity of the function are conflicting. Therefore, we can infer that the individual optimum will always be at the frontier of the spherical region.

375 Developing a correlation analysis for the 10 original responses as shown in Table 6, the values in bold represent the p-value for the immediately above mentioned Pearson correlation. Since the correlation between each pair of variables is high, a factor analysis to obtain uncorrelated factors was performed, which also provides an optimization problem with a reduced number of responses. Ini-

1  
2  
3  
4  
5  
6  
7  
8  
9 tially, it was considered 10 output variables ( $y_i$ ) and after performing the factor  
10 analysis we deal with only 3 factors ( $F_j$ ) that represent the original responses.  
11  
12

Table 6: Correlation matrix for the original responses

	HI	P	PA	D	W	R	CI	RA	PSF
P	0.070								
	<b>0.708</b>								
PA	0.600	0.800							
	<b>0.000</b>	<b>0.000</b>							
D	-0.243	0.818	0.523						
	<b>0.188</b>	<b>0.000</b>	<b>0.003</b>						
W	0.969	0.220	0.715	-0.127					
	<b>0.000</b>	<b>0.234</b>	<b>0.000</b>	<b>0.496</b>					
R	0.562	-0.387	0.038	-0.773	0.522				
	<b>0.001</b>	<b>0.032</b>	<b>0.841</b>	<b>0.000</b>	<b>0.003</b>				
CI	-0.529	-0.601	-0.738	-0.584	-0.615	0.335			
	<b>0.002</b>	<b>0.000</b>	<b>0.000</b>	<b>0.001</b>	<b>0.000</b>	<b>0.065</b>			
RA	0.891	-0.149	0.400	-0.542	0.872	0.854	-0.167		
	<b>0.000</b>	<b>0.425</b>	<b>0.026</b>	<b>0.002</b>	<b>0.000</b>	<b>0.000</b>	<b>0.369</b>		
PSF	0.635	-0.683	-0.150	-0.762	0.524	0.742	0.099	0.769	
	<b>0.000</b>	<b>0.000</b>	<b>0.420</b>	<b>0.000</b>	<b>0.002</b>	<b>0.000</b>	<b>0.595</b>	<b>0.000</b>	
RFF	0.564	0.597	0.767	-0.564	0.639	-0.316	-0.984	0.198	-0.089
	<b>0.001</b>	<b>0.000</b>	<b>0.000</b>	<b>0.001</b>	<b>0.000</b>	<b>0.084</b>	<b>0.000</b>	<b>0.286</b>	<b>0.632</b>

13  
14  
15  
16  
17  
18  
19  
20  
21  
22  
23  
24  
25  
26  
27  
28  
29  
30  
31  
32  
33  
34  
35  
36  
37  
38  
39  
40  
41  
42  
43  
44  
45  
46  
47  
48  
49  
50  
51  
52  
53  
54  
55  
56  
57  
58  
59  
60  
61  
62  
63  
64  
65

The factor analysis considers that one factor may represent many distinct variables, and the original ones are not used anymore and it is, henceforth, considered uncorrelated scores able to explain the original variables. The dendrogram shown in Fig. 6 indicates how the variables were clustered. It was considered the correlation as the distance measure and the ward linkage method to define the clusters.

Afterwards, the 10 original variables were replaced by the 3 uncorrelated

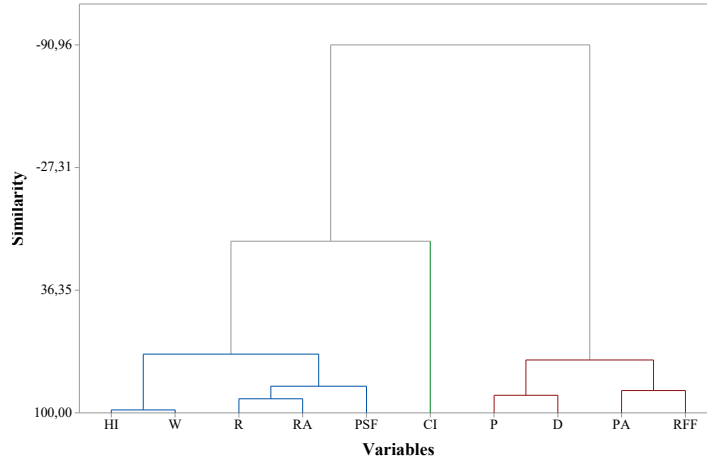


Figure 6: Dendrogram for the clustered variables

factors. They were extracted by correlation and using varimax rotation type, as suggested by (Almeida et al., 2020).

390 It can be viewed in Table 7 the sorted rotated factor loadings and communalities, where the loading represent the correlation between the considered variable and the factor  $F_j$  and the communalities indicate the amount of its variability that is explained by the factors. Hence, it is possible to observe that 98% of the variance can be explained after performing the factor analysis.

395 Factor 1 represents the 5 variables (RA, R, HI, W, and PSF) which have the greatest loadings associated to this factor. Factor 2 comprises only one variable (CI) and factor 3 represents 4 variables (P, PA, RFF and D). In some cases they present conflicting optimization directions. Hence, in order to avoid the decision of maximizing or minimizing the factors, we worked here with MMSE as defined  
400 in Eq. (17), since the minimization is always adequate for this metric.

In the optimization the NBI method was applied to find optimal equidistant solutions in the Pareto surface, considering an array of 70 combinations of weights ranging from 0.00001 to 0.99998. This mixture design was generated through a simplex lattice mixture design with three components, degree of

Table 7: Sorted rotate loadings and communalities

Variable	Factor1	Factor2	Factor3	Communality
RA	0.986	-0.122	-0.072	0.993
R	0.904	0.385	-0.154	0.989
HI	0.847	-0.507	0.001	0.974
W	0.829	-0.534	0.151	0.995
PSF	0.727	-0.056	-0.654	0.959
CI	-0.073	0.941	-0.305	0.984
RFF	0.106	-0.938	0.315	0.99
P	-0.126	-0.341	0.925	0.988
PA	0.395	-0.527	0.739	0.979
D	-0.557	-0.461	0.651	0.947
Variance	4.2205	3.0797	2.4976	9.7978
% Var	0.422	0.308	0.25	0.98

lattice equals to 10, and augmented with the center and the axial points. The MMSE value for the 3 factors were considered as the responses to be minimized, since we desire an error value as close as possible to zero. Each combination of weights can be considered as a sub-problem of the NBI method, leading to 70 sub-problems. The 3D plot of the normalized factors and their respective weights are depicted in Fig. 7.

It was calculated, in each sub-problem, the value of the Mahalanobis' distance ( $D$ ) and the entropy ( $E$ ), according to Eq. (29) and Eq. (30), and these metrics were modelled and validated through ANOVA.

$$D = \sqrt{(\mathbf{x} - \mathbf{T})' \Sigma^{-1} (\mathbf{x} - \mathbf{T})} \quad (29)$$

$$E = - \sum_{j=1}^n w_j \ln(w_j) \quad (30)$$

where  $\mathbf{x}$  is the vector of the original variables values and  $\mathbf{T}$  is the vector of targets associated to them. Regarding the entropy equation,  $w_j$  represents the

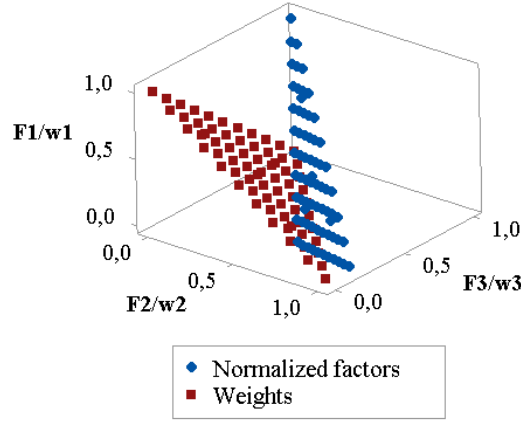


Figure 7: 3D plot of the normalized factors versus their respective weights

$j$ -th value of weight considered in each sub-problem of the NBI.

The model for the Mahalanobis' distance can be viewed in Eq. (31), with  $R^2$  and  $R^2_{adj}$  equal to 76.11% and 74.25%, respectively. Regarding the entropy, Eq. (32) shows its model with  $R^2$  and  $R^2_{adj}$  equal to 95.82% and 95.50%, respectively.

$$D = 5.627w_1 + 7.272w_2 + 6.057w_3 - 15.266w_1w_2 - 14.883w_1w_3 - 16.860w_2w_3 \quad (31)$$

$$E = 0.001(w_1 + w_2 + w_3) + 3.241w_1w_2 + 3.241w_1w_3 + 3.241w_2w_3 \quad (32)$$

The contour and surface plot for both are shown in Fig. 8 and Fig. 9, respectively. As it can be observed, the convexity and optimization directions are coincident.

For the 70 combinations of weights it was calculated the ratio between the entropy and the Mahalanobis' distance. The ratio reached its maximum value 0.8272 when  $w_1 = 0.30$ ,  $w_2 = 0.30$ , and  $w_3 = 0.40$ , representing the best point of the Pareto's surface previously constructed. Optimizing the MMSE functions



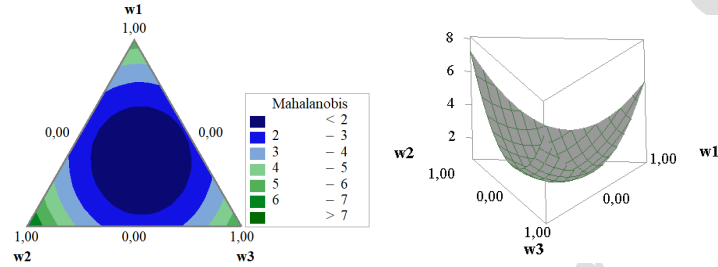


Figure 8: Contour and surface plot for Mahalanobis' distance

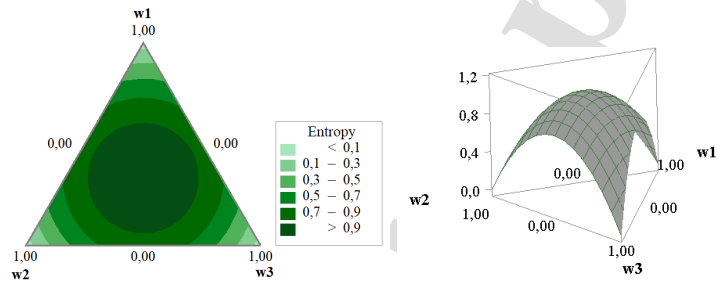


Figure 9: Contour and surface plot for entropy

considering this set of weights, the following values for the original 10 variables are obtained, as shown in Table 8. Also, it is presented the individual targets for each variable and the value obtained using the Desirability algorithm.

Nevertheless it is important to highlight that even though the Desirability optimal values seem to be better, they violate the experimental region, since the algorithm does not contemplate this constraint. It indicates the coded values 2.00, 1.64, -1.23, and 2.00 for the input variables WFR, AV, WS, and CTWD, respectively, meaning that  $\mathbf{x}'\mathbf{x}$  results in 12.19, which is much greater than the  $\rho^2 = 4$ .

Figure 10 was built simultaneously considering the feasible region for all the mathematical models generated for each original response variable and for the 3 extracted factors. It shows that the optimal solution identified by the red point relies on the blank area that comprises the global problem's feasible region. Then, it is easy to verify, by observing Table 8 and Figure 10, the complexity of

Table 8: Optimized responses and individual targets for the output variables

	Optimized response	Individual target	Desirability optimal values
HI	1.4300	0.4371	1.3990
P	1.2901	0.8320	0.7151
PA	9.7068	4.6846	9.1794
D	0.2310	0.1664	0.2213
W	14.1002	15.5248	15.6032
R	3.1701	3.5221	3.5256
CI	0.2205	0.1797	0.2508
RA	33.1815	38.5868	37.3566
PSF	11.8559	14.5843	15.4382
RFF	4.4722	5.3035	4.3546

a multiobjective problem with many variables and the trade-off situation while optimizing the functions.

The optimized values from TPO - Phase 1 indicate that the best weld bead may be obtained by setting the input variables with the following uncoded values: WFR = 8.96m/min, AV = 29,38V, WS = 24.21cm/min and CTWD = 17.90mm.

## 5.2. Optimization of the cladding process focusing on the reduction of the energy and material

### 5.2.1. Brazilian electrical charging system

The energy cost in Brazil is based on a distinct electrical charging system. It consists on two portions, here called electrical energy consumption (kW/h) and active power demand (kW), according to the supply mode. This system also contemplates a segment based on time-season, that assigns different fees for the "peak hours" (PH) and "off-peak hours" (OPH). PH refers to the period of three daily consecutive hours, from 6p.m. to 9p.m., established by the energy provider. On the other hand, OPH are the daily consecutive hours that comple-

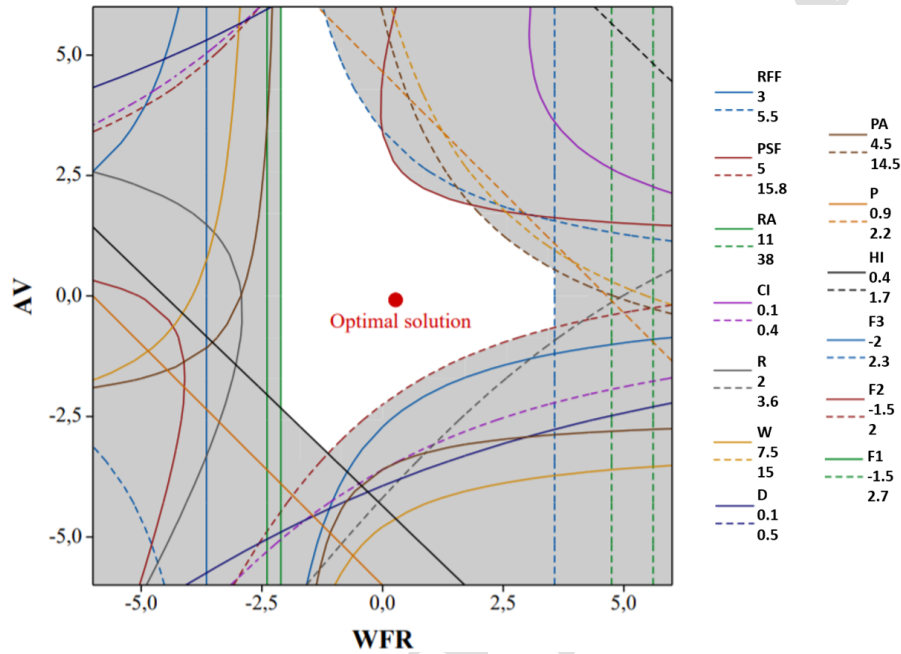


Figure 10: Overlaid contour plot for the original variables and the factors

ment the PH. Besides that, there are some distinct values for a period of seven cycles of consecutive invoices, between May and November - the "dry period" -, and for the period of five cycles of consecutive invoices, between December and April of the next year - the "wet period".

There are three available provision categories: standard, green hour and blue hour. The first one is the traditional binomial charging modality with a minimum of 30kW and a maximum of 149kW contracted demand, and whose fees for the electrical energy consumption and power demand do not depend on the period of usage. The green hour modality consists on differentiated fees for the electrical energy consumption according to the period of the day and the month (dry/wet), and a unique fee for the power demand, with a 30kW minimal contracted demand. The last one, blue hour, contemplates different fees for both electrical energy consumption and the power demand, according to the period of usage, with a 30kW minimal contracted demand, for PH or

OPH. The consumers that may opt for one of these 3 categories must have an installed power between 30kW and 300kW (this value may change depending on the specific energy provider).

475 The Tariff Flags System is another important characteristic from the Brazilian charging system that was incorporated in 2015. It determines whether there will be an extra energy cost to the final consumer, according to the energy generation condition, as shown in Table 9.

Table 9: Brazilian Tariff Flag System

Flag	Description
Green	Favorable energy generation conditions. There is no modification in the energy cost.
Yellow	Less favorable energy generation conditions. A fee of \$0.0025 is added to every consumed kWh.
Red - Level 1	More costly energy generation conditions. A fee of \$0.0075 is added to every consumed kWh.
Red - Level 2	Still more costly energy generation conditions. A fee of \$0.0125 is added to every consumed kWh.

Table 10 shows the tariffs obtained from an specific energy provider to be considered in this case, according to the blue hour category, and refers to a determined month (March, 2019). These values can be monthly modified due to the energetic context of the country in terms of production and consumption.

Table 10: Flag values for dry and wet periods

	Green	Yellow	Red - Level 1	Red - Level 2
PH - Dry	0.080705	0.083205	0.088205	0.093205
PH - Wet	0.080705	0.083205	0.088205	0.093205
OPH - Dry	0.1193825	0.1218825	0.1268825	0.1318825
OPH - Wet	0.1193825	0.1218825	0.1268825	0.1318825

Considering the information from Table 10 and the previously presented

1  
2  
3  
4  
5  
6  
7  
8  
9 data, Tables 11 and 12 detail the energy cost for OPH and PH, respectively,  
10  
11 485 calculated from the heat input of every considered experiment.  
12

13 Table 11: Energy cost from the heat input for the OPH  
14

#	WFR	AV	WS	CTWD	Green	Yellow	Red L1	Red L2
1	7	27	30	15	0.075	0.077	0.082	0.087
2	10	27	30	15	0.093	0.096	0.102	0.108
3	7	32	30	15	0.093	0.096	0.102	0.108
4	10	32	30	15	0.120	0.124	0.132	0.139
5	7	27	50	15	0.045	0.047	0.049	0.052
6	10	27	50	15	0.054	0.055	0.059	0.062
7	7	32	50	15	0.055	0.056	0.060	0.063
8	10	32	50	15	0.068	0.070	0.074	0.078
9	7	27	30	25	0.062	0.064	0.068	0.072
10	10	27	30	25	0.078	0.080	0.085	0.090
11	7	32	30	25	0.079	0.081	0.086	0.091
12	10	32	30	25	0.092	0.095	0.101	0.107
13	7	27	50	25	0.037	0.039	0.041	0.043
14	10	27	50	25	0.046	0.048	0.051	0.053
15	7	32	50	25	0.047	0.048	0.051	0.054
16	10	32	50	25	0.057	0.058	0.062	0.065
17	5.5	29.5	40	20	0.050	0.052	0.055	0.058
18	11.5	29.5	40	20	0.076	0.078	0.083	0.088
19	8.5	24.5	40	20	0.052	0.054	0.057	0.060
20	8.5	34.5	40	20	0.079	0.081	0.086	0.091
21	8.5	29.5	20	20	0.134	0.138	0.146	0.154
22	8.5	29.5	60	20	0.041	0.042	0.045	0.047
23	8.5	29.5	40	10	0.080	0.082	0.087	0.092
24	8.5	29.5	40	30	0.054	0.056	0.059	0.063

Table 11 continued from previous page

25	8.5	29.5	40	20	0.064	0.066	0.070	0.074
26	8.5	29.5	40	20	0.065	0.067	0.071	0.075
27	8.5	29.5	40	20	0.064	0.066	0.070	0.074
28	8.5	29.5	40	20	0.063	0.065	0.069	0.073
29	8.5	29.5	40	20	0.062	0.064	0.068	0.072
30	8.5	29.5	40	20	0.061	0.063	0.067	0.071
31	8.5	29.5	40	20	0.062	0.064	0.068	0.072

Table 12: Energy cost from the heat input for the PH

#	WFR	AV	WS	CTWD	Green	Yellow	Red L1	Red L2
1	7	27	30	15	0.111	0.113	0.118	0.122
2	10	27	30	15	0.138	0.141	0.147	0.152
3	7	32	30	15	0.138	0.141	0.147	0.153
4	10	32	30	15	0.178	0.182	0.189	0.197
5	7	27	50	15	0.067	0.068	0.071	0.074
6	10	27	50	15	0.079	0.081	0.084	0.088
7	7	32	50	15	0.081	0.082	0.086	0.089
8	10	32	50	15	0.100	0.102	0.106	0.110
9	7	27	30	25	0.092	0.094	0.098	0.102
10	10	27	30	25	0.115	0.118	0.123	0.127
11	7	32	30	25	0.116	0.119	0.123	0.128
12	10	32	30	25	0.137	0.140	0.145	0.151
13	7	27	50	25	0.055	0.056	0.059	0.061
14	10	27	50	25	0.068	0.070	0.073	0.076
15	7	32	50	25	0.069	0.071	0.074	0.076
16	10	32	50	25	0.084	0.086	0.089	0.093
17	5.5	29.5	40	20	0.074	0.076	0.079	0.082

Table 12 continued from previous page

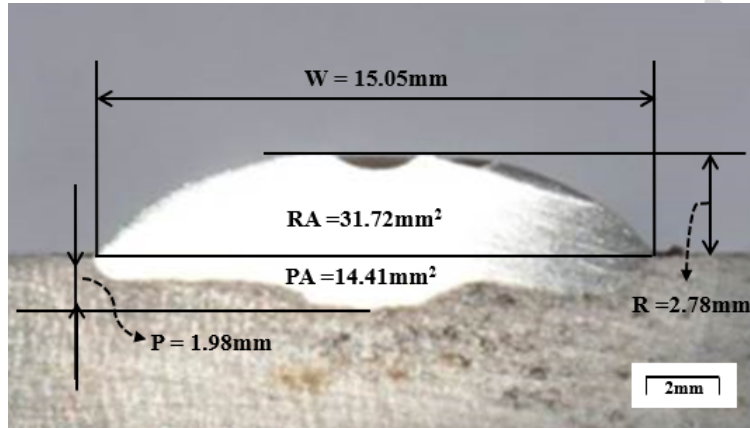
18	11.5	29.5	40	20	0.113	0.115	0.120	0.124
19	8.5	24.5	40	20	0.077	0.078	0.082	0.085
20	8.5	34.5	40	20	0.116	0.119	0.123	0.128
21	8.5	29.5	20	20	0.198	0.202	0.210	0.218
22	8.5	29.5	60	20	0.061	0.062	0.064	0.067
23	8.5	29.5	40	10	0.118	0.120	0.125	0.130
24	8.5	29.5	40	30	0.080	0.082	0.085	0.089
25	8.5	29.5	40	20	0.095	0.097	0.101	0.105
26	8.5	29.5	40	20	0.096	0.098	0.102	0.106
27	8.5	29.5	40	20	0.095	0.097	0.101	0.104
28	8.5	29.5	40	20	0.093	0.095	0.099	0.103
29	8.5	29.5	40	20	0.092	0.094	0.098	0.102
30	8.5	29.5	40	20	0.091	0.093	0.097	0.100
31	8.5	29.5	40	20	0.092	0.094	0.098	0.102

### 5.2.2. Multiobjective stochastic optimization

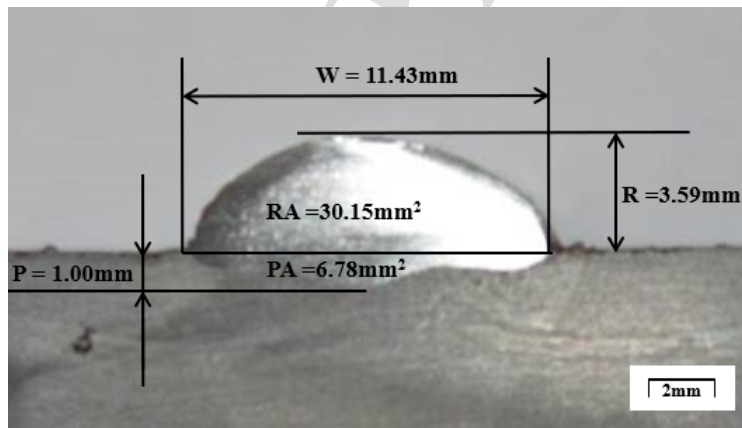
The heat input and the reinforcement, in this paper, were chosen as the two most relevant responses regarding an environmental approach, since they are related to the energy consumption and the rework, respectively. Therefore, a second approach is proposed based on a multiobjective stochastic optimization. The purpose is to minimize the sum of the expected value for the excess and lack of material (stainless steel) and its associated variance, subjected to a specified value of energy cost.

When adding more material than it is really necessary, a machining process will be indispensable to remove the excess and to improve the characteristics of the surface. In cases of depositing less material than expected, another welding process will be required to fulfill the demanded amount. For both scenarios, we must consider the optimum bead geometry obtained from TPO - Phase 1 as the target. In order to calculate the relevant areas, the original photos, Fig. 11 to

1  
2  
3  
4  
5  
6  
7  
8  
9  
500 Fig. 14, were converted into images through which it was possible to identify  
10 these values.  
11



28 Figure 11: Original photo of the 4-th experimental weld bead



47 Figure 12: Original photo of the 10-th experimental weld bead

48  
49  
50  
51  
52  
53  
54  
55  
56  
505  
57  
58  
59  
60  
61  
62  
63  
64  
65

Figures 15 to 18 shows the images of the same weld beads presented on Fig. 11 to Fig. 14, but converted into images where the blue and red area represent the scrap and rework, respectively, when compared to the optimum weld bead geometry. These figures were obtained using a computer graphics software (Paes, 2020) where the real photos were converted into images to make



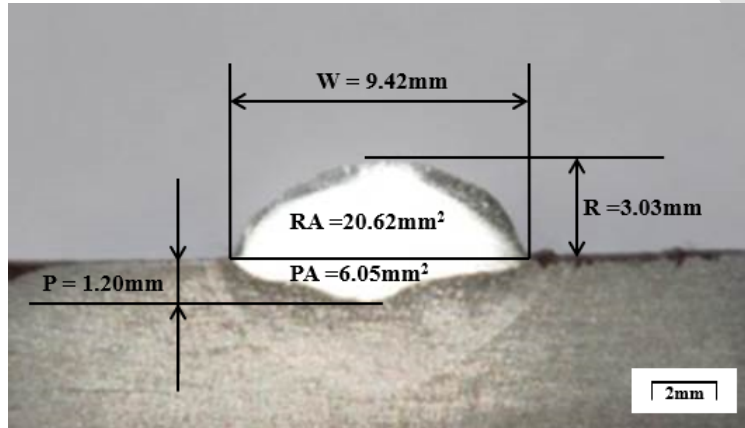


Figure 13: Original photo of the 19-th experimental weld bead

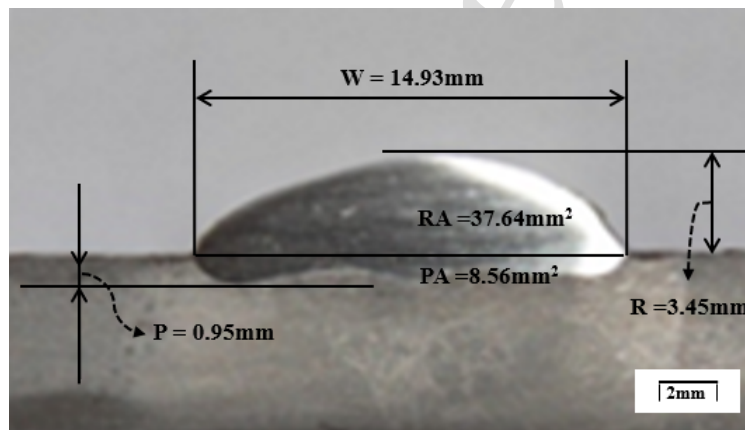


Figure 14: Original photo of the 21-st experimental weld bead

it possible to count the pixels to calculate the real measures. The scrap and the rework areas were jointly considered in the problem, and they are referred to as rework.

510 The other aspect in the stochastic programming refers to the cost related to the energy used in the welding process. It was applied a constraint which implies that the cost value will not exceed \$0.10, with a probability of 97.5%.

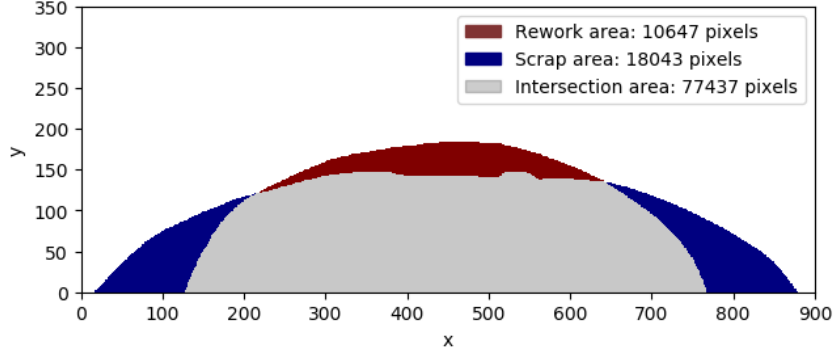


Figure 15: Scrap and rework areas of the 4-th experimental weld bead

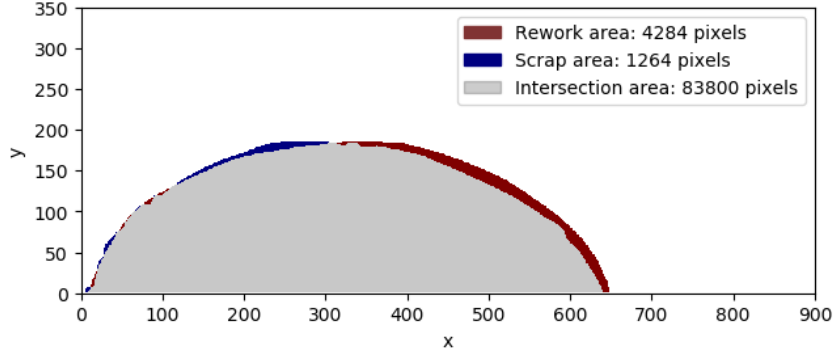


Figure 16: Scrap and rework areas of the 10-th experimental weld bead

Hence the modelling of the problem can be viewed in Eq. (33).

$$\begin{aligned}
 \min_x F(x) &= w_1(\mathbf{Z}(\mathbf{x})'\beta) + (1 - w_1)[\sigma^2\mathbf{Z}(\mathbf{x})'(\mathbf{X}'\mathbf{X})^{-1}\mathbf{Z}(\mathbf{x})] \\
 s.t. \quad g_1(\mathbf{x}) &= \mathbf{Z}(\mathbf{x})'\gamma + s_i\sigma\sqrt{\mathbf{Z}(\mathbf{x})'(\mathbf{X}'\mathbf{X})^{-1}\mathbf{Z}(\mathbf{x})} \leq 0.1 \\
 g_2(\mathbf{x}) &= \mathbf{x}'\mathbf{x} \leq 4
 \end{aligned} \tag{33}$$

where  $\sigma^2$  is the Mean Square Error (MSE) obtained through the analysis of variance,  $s_i$  is equal to 1.96 which represents a probability equals to 97.5%, and, finally,  $\beta$  and  $\gamma$  are the vectors containing the coefficients of the model for the rework and for the energy cost, respectively. Applying the NBI method once

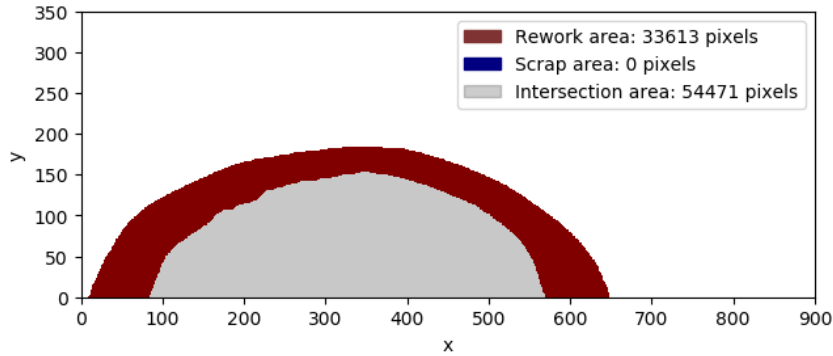


Figure 17: Scrap and rework areas of the 19-th experimental weld bead

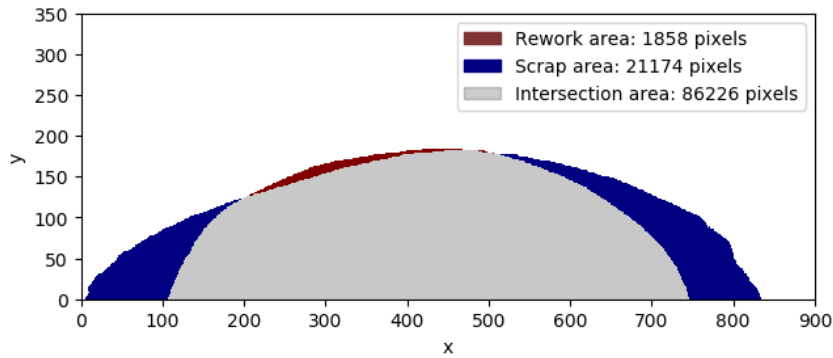


Figure 18: Scrap and rework areas of the 21-st experimental weld bead

more, the Pareto frontier depicted in Fig. 19 is obtained.

In order to find the best point of the frontier, it was used the Mahalanobis' distance as the evaluation criterion. Table 13 presents the values for the process parameters, the optimal results, the Mahalanobis' distance, and the energy cost for each NBI subproblem.

It is possible to observe that the point which presents the smaller value for the Mahalanobis' distance is the 15th. Considering this point, the values for the input parameters in coded units are  $WFR = 0.967$ ,  $AV = -0.600$ ,  $WS = -0.649$  e  $CTWD = 1.081$ . Therefore, their values in uncoded units are  $WFR = 9.95\text{m/min}$ ,  $AV = 28.00\text{V}$ ,  $WS = 33.51\text{cm/min}$  and  $CTWD =$

Table 13: Optimal values for the stochastic problem

#	w	WFR	AV	WS	CTWD	Rework		Mahalanobi's distance	Energy cost
						Mean	Variance		
1	0.00	8.5	29.5	40.0	20.0	11.273	0.094	2.898	0.342
2	0.05	8.6	29.5	39.0	22.3	10.322	0.094	2.037	0.340
3	0.10	8.7	29.4	37.6	22.5	9.533	0.099	1.480	0.355
4	0.15	8.9	29.4	36.4	22.7	8.829	0.108	1.141	0.371
5	0.20	9.0	29.3	35.4	22.9	8.192	0.119	1.008	0.380
6	0.25	9.1	29.3	34.4	23.0	7.648	0.133	1.039	0.380
7	0.30	9.2	29.0	34.1	23.5	7.182	0.150	1.122	0.380
8	0.35	9.4	28.8	34.0	23.8	6.772	0.169	1.163	0.380
9	0.40	9.5	28.7	33.9	24.1	6.404	0.189	1.153	0.380
10	0.45	9.6	28.5	33.8	24.4	6.071	0.211	1.098	0.380
11	0.50	9.7	28.4	33.7	24.7	5.765	0.233	1.009	0.380
12	0.55	9.7	28.3	33.6	24.9	5.482	0.257	0.901	0.380
13	0.60	9.8	28.2	33.6	25.1	5.218	0.281	0.795	0.380
14	0.65	9.9	28.1	33.5	25.2	4.970	0.306	0.721	0.380
15	0.70	10.0	28.0	33.5	25.4	4.737	0.331	0.718	0.380
16	0.75	10.0	27.9	33.5	25.6	4.515	0.356	0.809	0.380
17	0.80	10.1	27.9	33.4	25.7	4.305	0.382	0.986	0.380
18	0.85	10.1	27.8	33.4	25.8	4.105	0.409	1.223	0.380
19	0.90	10.2	27.7	33.4	26.0	3.913	0.435	1.501	0.380
20	0.95	10.2	27.7	33.4	26.1	3.728	0.462	1.809	0.380
21	1.00	10.3	27.6	33.4	26.2	3.551	0.490	2.139	0.380

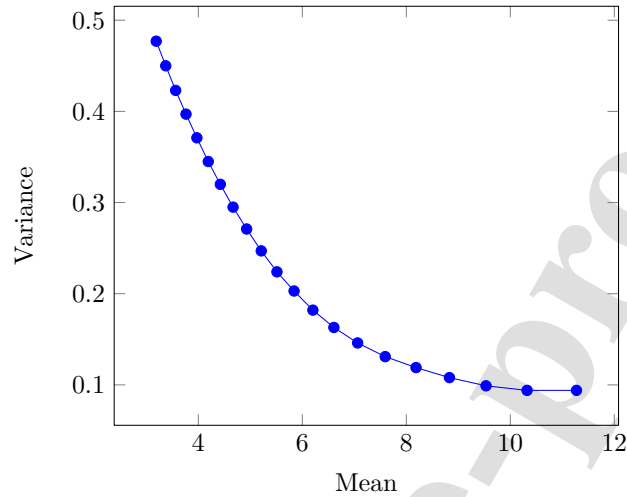


Figure 19: Pareto's Frontier for the material involved in the rework process

25.41mm, determining the optimal setting for the sustainability approach involving both energy cost and rework.

530 We applied the Generalized Reduced Gradient with convergency equal to  $10^{-6}$ . Figure 20 was plotted from the values of the objective function for all the iterations of the second NBI subproblem.

Some of the main results achieved in this article regarding both quality and sustainability scenarios are summarized in Table 14.

## 535 6. Conclusion

Several real optimization problems are classified as multiobjective and may present a large number of responses with conflicting objectives. To deal with this, this paper presented a Two-Phased Optimization Methodology (TPO) applying Factor Analysis, Normal Boundary Intersection (NBI), and the Multi-  
540 variate Mean Square Error (MMSE). After modelling the responses using the Response Surface Methodology (RSM), the first stage consisted in minimizing the MMSE related to the factors that represented the original objective functions. In the second stage a multiobjective stochastic optimization problem was

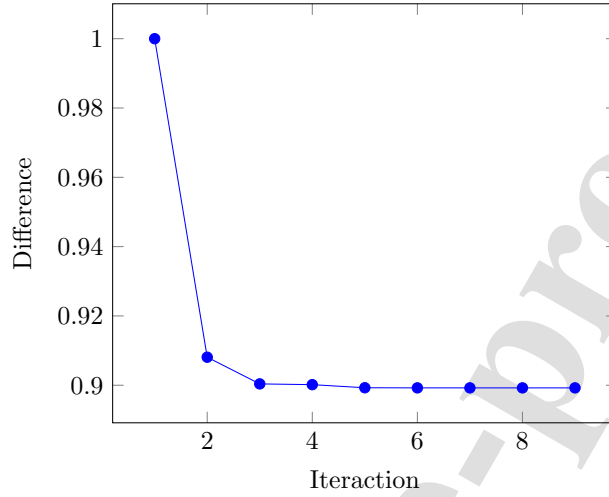


Figure 20: Convergence of the GRG algorithm for the second NBI subproblem

Table 14: Table of parameters and optimized responses

	Quality scenario	Sustainability scenario
	WFR = 8.96 AV = 29.38	WFR = 9.95 AV = 28.00
	WS = 24.21 CTWD = 17.90	WS = 33.51 CTWD = 25.41
HI	1.4300	0.9054
P	1.2901	1.1547
PA	9.7068	6.9210
D	0.2310	0.2160
W	14.1002	11.2695
R	3.1701	3.2635
CI	0.2205	0.2963
RA	33.1815	27.1925
PSF	11.8559	9.9239
RFF	4.4722	3.3537

modelled considering the most relevant original responses for the researcher,  
 545 aiming to approximate them even more to the target without harming the so-

1  
2  
3  
4  
5  
6  
7  
8  
9 lution obtained in TPO - Phase 1.

10 This methodology was applied in a multiobjective cladding process of ABNT  
11 1020 carbon steel plate using austenitic ABNT 316L stainless steel cored wire.  
12 The experiments were conducted by RSM and the first phase focused on the  
13  
14 The product quality, optimizing the geometric characteristics of the weld bead. The  
15 550 second phase gave more importance to the process sustainability, solving a mul-  
16 tiobjective stochastic problem aiming the minimization of the material involved  
17 in the rework process jointly with the energy consumption.  
18  
19

20 Hence, it was possible to state that the methodology provides consistent  
21  
22 555 results when dealing with a large number of responses, considering both quality  
23 and environmental aspects.  
24  
25  
26

## 27 **Acknowledgment**

28  
29 The authors would like to thank the Brazilian agencies of CAPES, CNPq  
30 and FAPEMIG for supporting this research.  
31  
32  
33

## 34 560 **References**

### 35 **References**

36  
37 Almeida, F., Streitenberger, S., Torres, A., Paiva, A., Gomes, J., 2020. A gage  
38 study through the weighting of latent variables under orthogonal rotation.  
39 IEEE Access 8, 183557–183570.  
40  
41

42  
43 565 Baghel, R., Upadhyaya, S., Chaurasia, S.P., Singh, K., Kalla, S., 2018. Opti-  
44 mization of process variables by the application of response surface method-  
45 ology for naphthol blue black dye removal in vacuum membrane distillation.  
46 Journal of Cleaner Production 199, 900–915.  
47  
48

49  
50 Bahrami, H., Eslami, A., Nabizadeh, R., Mohseni-Bandpi, A., Asadi, A., Sillan-  
51 paa, M., 2018. Degradation of trichloroethylene by sonophotolytic-activated  
52 persulfate processes: Optimization using response surface methodology. Jour-  
53 570 nal of Cleaner Production 198, 1210–1218.  
54  
55  
56  
57  
58

- 1  
2  
3  
4  
5  
6  
7  
8  
9 Box, G.E.P., Hunter, J.S., 1957. Multi-factor experimental designs for exploring  
10 response surfaces. *The Annals of Mathematical Statistics* 28, 195–241.
- 11  
12  
13 575 Box, G.E.P., Hunter, W.G., MacGregor, J.F., Erjavec, J., 1973. Some problems  
14 associated with the analysis of multiresponse data. *Technometrics* 15, 33–51.
- 15  
16  
17 Brito, T.G., Paiva, A.P., Ferreira, J.R., Gomes, J.H.F., Balestrassi, P.P., 2014.  
18 A normal boundary intersection approach to multiresponse robust optimization  
19 of the surface roughness in end milling process with combined arrays.  
20  
21 580 *Precision Engineering* 38, 628–638.
- 22  
23  
24 Cao, L., Chen, H., Tsang, D.C.W., Luo, G., Hao, S., Zhang, S., Chen, J.,  
25 2018. Optimizing xylose production from pinewood sawdust through dilute-  
26 phosphoric-acid hydrolysis by response surface methodology. *Journal of*  
27 *Cleaner Production* 178, 572–579.
- 28  
29  
30  
31 585 Charoen, K., Prapainainar, C., Sureeyatanapas, P., Suwannaphisit, T., Wong-  
32 amornpitak, K., Kongkachuichay, P., Holmes, S.M., Prapainainar, P., 2017.  
33 Application of response surface methodology to optimize direct alcohol fuel  
34 cell power density for greener energy production. *Journal of Cleaner Produc-*  
35 *tion* 142, 1309–1320.
- 36  
37  
38  
39 590 Choudhury, P., Mondal, P., Majumdar, S., Saha, S., Sahoo, G.C., 2018.  
40 Preparation of ceramic ultrafiltration membrane using green synthesized cuo  
41 nanoparticles for chromium (vi) removal and optimization by response surface  
42 methodology. *Journal of Cleaner Production* 203, 511–520.
- 43  
44  
45  
46  
47 Costa, D., Paula, T., Silva, P., Paiva, A., 2016a. Normal boundary intersection  
48 595 method based on principal components and taguchi's signal-to-noise ratio ap-  
49 plied to the multiobjective optimization of 12l14 free machining steel turning  
50 process. *International Journal of Advanced Manufacturing Technology* 87,  
51 825–834.
- 52  
53  
54  
55  
56  
57 600 Costa, D.M.D., Brito, T.G., Paiva, A.P., Leme, R.C., Balestrassi, P.P., 2016b. A  
58 normal boundary intersection with multivariate mean square error approach



- 1  
2  
3  
4  
5  
6  
7  
8  
9 for dry end milling process optimization of the aisi 1045 steel. *Journal of*  
10 *Cleaner Production* 135, 1658–1672.
- 11  
12  
13 Das, I., Dennis, J.E., 1998. Normal-boundary intersection: a new method for  
14 generating the pareto surface in nonlinear multicriteria optimization prob-  
15 lems. *SIAM Journal on Optimization* 8, 631–657.  
605
- 16  
17  
18 Díaz-García, J.A., Bshiri, M., 2014. Multiple response optimization: An ap-  
19 proach from multiobjective stochastic programming. *Applied Mathematical*  
20 *Modelling* 38, 2015–2027.
- 21  
22  
23 Díaz-García, J.A., Ramos-Quiroga, R., Cabrera-Vicencio, E., 2005. Stochastic  
24 programming methods in the response surface methodology. *Computational*  
610 *Statistics and Data Analysis* 49, 837–848.
- 25  
26  
27  
28  
29 Flandinet, L., Tedjar, F., Ghetta, V., Fouletier, J., 2012. Metals recovering  
30 from waste printed circuit boards (WPCBs) using molten salts. *Journal of*  
31 *Hazardous Materials* 213-214, 485–490.
- 32  
33  
34  
615 Fu, Y., Tian, G., Fathollahi-Fard, A.M., Ahmadi, A., Zhang, C., 2019. Stochas-  
35 tic multi-objective modelling and optimization of an energy-conscious dis-  
36 tributed permutation flow shop scheduling problem with the total tardiness  
37 constraint. *Journal of Cleaner Production* 226, 515–525.
- 38  
39  
40  
41 Gasemloo, S., Khosravi, M., Sohrabi, M.R., Dastmalchi, S., Gharbani, P., 2019.  
42 Response surface methodology (rsm) modeling to improve removal of cr (vi)  
620 ions from tannery wastewater using sulfated carboxymethyl cellulose nanofil-  
43 ter. *Journal of Cleaner Production* 208, 736–742.
- 44  
45  
46  
47  
48 Gaudêncio, J., Almeida, F., Turrioni, J., Quinino, R., Balestrassi, P., Paiva,  
49 A., 2019. A multiobjective optimization model for machining quality in the  
50 aisi 12l14 steel turning process using fuzzy multivariate mean square error.  
625 *Precision Engineering* 56, 303–320.
- 51  
52  
53  
54  
55  
56  
57  
58  
59  
60  
61  
62  
63  
64  
65

- 1  
2  
3  
4  
5  
6  
7  
8  
9  
10  
11  
12  
13  
14  
15  
16  
17  
18  
19  
20  
21  
22  
23  
24  
25  
26  
27  
28  
29  
30  
31  
32  
33  
34  
35  
36  
37  
38  
39  
40  
41  
42  
43  
44  
45  
46  
47  
48  
49  
50  
51  
52  
53  
54  
55  
56  
57  
58  
59  
60  
61  
62  
63  
64  
65
- Gomes, J., Júnior, A., Paiva, A., Ferreira, J., Da Costa, S., Balestrassi, P., 2012. Global criterion method based on principal components to the optimization of manufacturing processes with multiple responses. *Strojnicki Vestnik/Journal of Mechanical Engineering* 58, 345–353.
- Gomes, J.H.F., Paiva, A.P., Costa, S.C., Balestrassi, P.P., Paiva, E.J., 2013. Weighted multivariate mean square error for processes optimization: A case study on flux-cored arc welding for stainless steel claddings. *European Journal of Operational Research* 226, 522–535.
- Gopal, K., Sathiyagnanam, A.P., Kumar, B.R., Saravanan, S., Rana, D., Sethuramasamyraja, B., 2018. Prediction of emissions and performance of a diesel engine fueled with n-octanol/diesel blends using response surface methodology. *Journal of Cleaner Production* 184, 423–439.
- Johnson, R.A., Wichern, D.W., 2007. *Applied multivariate statistical analysis*. 6th ed., Prentice Hall.
- Kakoi, B., Kaluli, J.W., Ndiba, P., Thiong'o, G., 2017. Optimization of maerua decumbent bio-coagulant in paint industry wastewater treatment with response surface methodology. *Journal of Cleaner Production* 164, 1124–1134.
- Khalid, A.A.H., Yaakob, Z., Abdullah, S.R.S., Takriff, M.S., 2019. Analysis of the elemental composition and uptake mechanism of *Chlorella sorokiniana* for nutrient removal in agricultural wastewater under optimized response surface methodology (rsm) conditions. *Journal of Cleaner Production* 210, 673–686.
- Klepa, R.B., Medeiros, M.F., Franco, M.A.C., Tamberg, E.T., Farias, T.M.B., Filho, J.A.P., Berssaneti, F.T., Santana, J.C.C., 2019. Reuse of construction waste to produce thermoluminescent sensor for use in highway traffic control. *Journal of Cleaner Production* 209, 250–258.
- Leite, R., 2019. Método de interseção normal à fronteira para modelos quadráticos de escores fatoriais rotacionais. Master's thesis. Federal University of Itajubá.

- 1  
2  
3  
4  
5  
6  
7  
8  
9  
10  
11  
12  
13  
14  
15  
16  
17  
18  
19  
20  
21  
22  
23  
24  
25  
26  
27  
28  
29  
30  
31  
32  
33  
34  
35  
36  
37  
38  
39  
40  
41  
42  
43  
44  
45  
46  
47  
48  
49  
50  
51  
52  
53  
54  
55  
56  
57  
58  
59  
60  
61  
62  
63  
64  
65
- 660 Liu, Z., Jiang, Q., Li, T., Dong, S., Yan, S., Zhang, H., Xu, B., 2016. Environmental benefits of remanufacturing: A case study of cylinder heads re-manufactured through laser cladding. *Journal of Cleaner Production* 133, 1027–1033.
- 665 Lu, Y., Xu, Z., 2017. Recycling non-leaching gold from gold-plated memory cards: Parameters optimization, experimental verification, and mechanism analysis. *Journal of Cleaner Production* 162, 1518–1526.
- Luz, E., Romao, E., Streitenberger, S., Gomes, J., Paiva, A., Balestrassi, P., 2021. A new multiobjective optimization with elliptical constraints approach for nonlinear models implemented in a stainless steel cladding process. *The International Journal of Advanced Manufacturing Technology* 113, 1469–1484.
- 670 Markandeya, Dhiman, N., Shukla, S.P., Kisku, G.C., 2017. Statistical optimization of process parameters for removal of dyes from wastewater on chitosan cenospheres nanocomposite using response surface methodology. *Journal of Cleaner Production* 149, 597–606.
- Mohammed, B.S., Khed, V.C., Nuruddin, M.F., 2018. Rubbercrete mixture optimization using response surface methodology. *Journal of Cleaner Production* 171, 1605–1621.
- 675 Mohammed, I.Y., Abakr, Y.A., Hui, J.N.X., Alaba, P.A., Morris, K.I., Ibrahim, M.D., 2017a. Recovery of clean energy precursors from bambara groundnut waste via pyrolysis: Kinetics, products distribution and optimisation using response surface methodology. *Journal of Cleaner Production* 164, 1430–1445.
- 680 Mohammed, I.Y., Abakr, Y.A., Yusup, S., Kazi, F.K., 2017b. Valorization of napier grass via intermediate pyrolysis: Optimization using response surface methodology and pyrolysis products characterization. *Journal of Cleaner Production* 142, 1848–1866.
- Montgomery, D.C., 2013. *Design and Analysis of Experiments*. 8th ed., John Wiley Sons, Inc.

- 1  
2  
3  
4  
5  
6  
7  
8  
9  
10  
11  
12  
13  
14  
15  
16  
17  
18  
19  
20  
21  
22  
23  
24  
25  
26  
27  
28  
29  
30  
31  
32  
33  
34  
35  
36  
37  
38  
39  
40  
41  
42  
43  
44  
45  
46  
47  
48  
49  
50  
51  
52  
53  
54  
55  
56  
57  
58  
59  
60  
61  
62  
63  
64  
65
- 685 Morero, B., Groppelli, E.S., Campanella, E.A., 2017. Evaluation of biogas  
upgrading technologies using a response surface methodology for process sim-  
ulation. *Journal of Cleaner Production* 141, 978–988.
- Nasiri, R., Arsalani, N., 2018. Synthesis and application of 3d graphene  
nanocomposite for the removal of cationic dyes from aqueous solutions: Re-  
690 sponse surface methodology design. *Journal of Cleaner Production* 190, 63–71.
- Osama, M., Walvekar, R., Khalid, M., Rasheed, A.K., Wong, W.Y., Gupta,  
T.C.S.M., 2018. Physical properties optimization of pome-groundnut-  
naphthenic based graphene nanolubricant using response surface methodol-  
ogy. *Journal of Cleaner Production* 193, 277–289.
- 695 Paes, V., 2020. Modelagem computacional aplicada à extração de características  
geométricas irregulares em processos multiobjetivos. Ph.D. thesis. Federal  
University of Itajubá.
- Paiva, A., Gomes, J., Peruchi, R., Leme, R., Balestrassi, P., 2014. A multivari-  
ate robust parameter optimization approach based on principal component  
700 analysis with combined arrays. *Computers and Industrial Engineering* 74,  
186–198.
- Paiva, A.P., Paiva, E.J., R., F.J., Balestrassi, P.P., Costa, S.C., 2009. A multi-  
variate mean square error optimization of aisi 52100 hardened steel turning.  
*International Journal of Advanced Manufacturing Technology* 43, 631–643.
- 705 Peng, S., Li, T., Li, M., Guo, Y., Shi, J., Tan, G.T., Zhang, H., 2019. An  
integrated decision model of restoring technologies selection for engine re-  
manufacturing practice. *Journal of Cleaner Production* 206, 598–610.
- Pereira, R., Leite, R., Alvim, A., Paiva, A., Ferreira, J., Davim, J., 2017. Multi-  
objective robust optimization of the sustainable helical milling process of the  
710 aluminum alloy al 7075 using the augmented-enhanced normalized normal  
constraint method. *Journal of Cleaner Production* 152, 474–496.

- 1  
2  
3  
4  
5  
6  
7  
8  
9 Pouladi, B., Fanaei, M.A., Baghmisheh, G., 2019. Optimization of oxidative  
10 desulfurization of gas condensate via response surface methodology approach.  
11 Journal of Cleaner Production 209, 965–977.  
12  
13  
14  
15 715 Ranic, M., Nikolic, M., Pavlovic, M., Buntic, A., Siler-Marinkovic, S.,  
16 Dimitrijevic-Brankovic, S., 2014. Optimization of microwave-assisted extrac-  
17 tion of natural antioxidants from spent espresso coffee grounds by response  
18 surface methodology. Journal of Cleaner Production 80, 69–79.  
19  
20  
21 Ren, C., Li, Z., Zhang, H., 2019. Integrated multi-objective stochastic fuzzy  
22 programming and ahp method for agricultural water and land optimization  
23 720 allocation under multiple uncertainties. Journal of Cleaner Production 210,  
24 12–24.  
25  
26  
27  
28 Rusinko, C., 2007. Green manufacturing: An evaluation of environmentally sus-  
29 sustainable manufacturing practices and their impact on competitive outcomes.  
30 IEEE Transactions on Engineering Management 54, 445–454.  
31 725  
32  
33 Shabani, N., Sowlati, T., 2016. A hybrid multi-stage stochastic programming-  
34 robust optimization model for maximizing the supply chain of a forest-based  
35 biomass power plant considering uncertainties. Journal of Cleaner Production  
36 112, 3285–3293.  
37  
38  
39  
40  
41 730 Shakourloo, A., 2017. A multi-objective stochastic goal programming model for  
42 more efficient remanufacturing process. International Journal of Advanced  
43 Manufacturing Technology 91, 1007–1021.  
44  
45  
46  
47 Simsek, B., Uygunoglu, T., Korucu, H., Kocakerim, M.M., 2018. Analysis of  
48 the effects of dioctyl terephthalate obtained from polyethylene terephthalate  
49 wastes on concrete mortar: A response surface methodology based desirability  
50 735 function approach application. Journal of Cleaner Production 170, 437–445.  
51  
52  
53 Sulaiman, N.S., Hashim, R., Amini, M.H.M., Danish, M., Sulaiman, O., 2018.  
54 Optimization of activated carbon preparation from cassava stem using re-  
55  
56  
57  
58  
59  
60  
61  
62  
63  
64  
65

- 1  
2  
3  
4  
5  
6  
7  
8  
9  
10  
11  
12  
13  
14  
15  
16  
17  
18  
19  
20  
21  
22  
23  
24  
25  
26  
27  
28  
29  
30  
31  
32  
33  
34  
35  
36  
37  
38  
39  
40  
41  
42  
43  
44  
45  
46  
47  
48  
49  
50  
51  
52  
53  
54  
55  
56  
57  
58  
59  
60  
61  
62  
63  
64  
65
- sponse surface methodology on surface area and yield. *Journal of Cleaner Production* 198, 1422–1430.
- 740 Tyagi, M., Rana, A., Kumari, S., Jagadevan, S., 2018. Adsorptive removal of cyanide from coke oven wastewater onto zero-valent iron: Optimization through response surface methodology, isotherm and kinetic studies. *Journal of Cleaner Production* 178, 398–407.
- 745 Uddin, M.K., Baig, U., 2019. Synthesis of  $\text{Co}_3\text{O}_4$  nanoparticles and their performance towards methyl orange dye removal: Characterisation, adsorption and response surface methodology. *Journal of Cleaner Production* 211, 1141–1153.
- Venkatakrishnan, B., Sandhya, K.V., Abinandan, S., Vedaraman, N., Velappan, K.C., 2019. Fixation of carbon dioxide and optimization of liming process waste produced in tanneries using response surface methodology. *Journal of Cleaner Production* 209, 855–861.
- 750 Wang, C., Wang, H., Liu, Y., Huang, L., 2016. Optimization of surface treatment for flotation separation of polyvinyl chloride and polyethylene terephthalate waste plastics using response surface methodology. *Journal of Cleaner Production* 139, 866–872.
- 755 Wu, F., 2004. Optimization of correlated multiple quality characteristics using desirability function. *Quality Engineering* 17, 119–126.
- Yang, Z., Liu, P., Cheng, L., Wang, H., Ming, B., Gong, W., 2018. Deriving operating rules for a large-scale hydro-photovoltaic power system using implicit stochastic optimization. *Journal of Cleaner Production* 195, 562–572.
- 760 Yuan, J., Wang, K., Yu, T., Fang, M., 2008. Reliable multi-objective optimization of high-speed wedm process based on gaussian process regression. *International Journal of Machine Tools Manufacture* 48, 47–60.
- Zbair, M., Ahsaine, H.A., Anfar, Z., 2018. Porous carbon by microwave assisted pyrolysis: An effective and low-cost adsorbent for sulfamethoxazole adsorp-
- 765

tion and optimization using response surface methodology. *Journal of Cleaner Production* 202, 571–581.

Zhang, P., Liu, Z., 2017. On sustainable manufacturing of cr-ni alloy coatings by laser cladding and high-efficiency turning process chain and consequent corrosion resistance. *Journal of Cleaner Production* 161, 676–687.

## Appendix A

Table A.1 - Investigated articles

Authors	Title
(Ranic et al., 2014)	Optimization of microwave-assisted extraction of natural antioxidants from spent espresso coffee grounds by response surface methodology
(Sarıkaya and Gullu, 2014)	Taguchi design and response surface methodology based analysis of machining parameters in CNC turning under MQL
(Wang et al., 2016)	Optimization of surface treatment for flotation separation of polyvinyl chloride and polyethylene terephthalate waste plastics using response surface methodology
(Charoen et al., 2017)	Application of response surface methodology to optimize direct alcohol fuel cell power density for greener energy production
(Kakoi et al., 2017)	Optimization of Maerua Decumbent bio-coagulant in paint industry wastewater treatment with response surface methodology

Table A.1 continued from previous page

(Markandeya et al., 2017)	Statistical optimization of process parameters for removal of dyes from wastewater on chitosan cenospheres nanocomposite using response surface methodology
(Mohammed et al., 2017a)	Recovery of clean energy precursors from Bambara groundnut waste via pyrolysis: Kinetics, products distribution and optimisation using response surface methodology
(Mohammed et al., 2017b)	Valorization of Napier grass via intermediate pyrolysis: Optimization using response surface methodology and pyrolysis products characterization
(Morero et al., 2017)	Evaluation of biogas upgrading technologies using a response surface methodology for process simulation
(Baghel et al., 2018)	Optimization of process variables by the application of response surface methodology for naphthol blue black dye removal in vacuum membrane distillation
(Bahrami et al., 2018)	Degradation of trichloroethylene by sonophotolytic-activated persulfate processes: Optimization using response surface methodology
(Cao et al., 2018)	Optimizing xylose production from pinewood sawdust through dilute-phosphoric-acid hydrolysis by response surface methodology
(Choudhury et al., 2018)	Preparation of ceramic ultrafiltration membrane using green synthesized CuO nanoparticles for chromium (VI) removal and optimization by response surface methodology



Table A.1 continued from previous page

(Gopal et al., 2018)	Prediction of emissions and performance of a diesel engine fueled with n-octanol/diesel blends using response surface methodology
(Mohammed et al., 2018)	Rubbercrete mixture optimization using response surface methodology
(Nasiri and Arsalani, 2018)	Synthesis and application of 3D graphene nanocomposite for the removal of cationic dyes from aqueous solutions: Response surface methodology design
(Osama et al., 2018)	Physical properties optimization of POME-groundnut-naphthenic based graphene nanolubricant using response surface methodology
(Simsek et al., 2018)	Analysis of the effects of dioctyl terephthalate obtained from polyethylene terephthalate wastes on concrete mortar: A response surface methodology based desirability function approach application
(Sulaiman et al., 2018)	Optimization of activated carbon preparation from cassava stem using response surface methodology on surface area and yield
(Tyagi et al., 2018)	Adsorptive removal of cyanide from coke oven wastewater onto zero-valent iron: Optimization through response surface methodology, isotherm and kinetic studies
(Zbair et al., 2018)	Porous carbon by microwave assisted pyrolysis: An effective and low-cost adsorbent for sulfamethoxazole adsorption and optimization using response surface methodology

Table A.1 continued from previous page

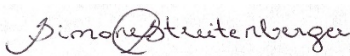
(Gasemloo et al., 2019)	Response surface methodology (RSM) modeling to improve removal of Cr (VI) ions from tannery wastewater using sulfated carboxymethyl cellulose nanofilter
(Khalid et al., 2019)	Analysis of the elemental composition and uptake mechanism of <i>Chlorella sorokiniana</i> for nutrient removal in agricultural wastewater under optimized response surface methodology (RSM) conditions
(Pouladi et al., 2019)	Optimization of oxidative desulfurization of gas condensate via response surface methodology approach
(Uddin and Baig, 2019)	Synthesis of Co <sub>3</sub> O <sub>4</sub> nanoparticles and their performance towards methyl orange dye removal: Characterisation, adsorption and response surface methodology
(Venkatakrisnan et al., 2019)	Fixation of carbon dioxide and optimization of liming process waste produced in tanneries using response surface methodology

Simone C. Streitenberger: Conceptualization, Methodology, Formal analysis, Investigation, Writing - Original Draft, Writing - Review & Editing, Visualization. Estevão L. Romão: Conceptualization, Methodology, Formal analysis, Investigation, Writing - Original Draft, Writing - Review & Editing, Visualization. Anderson P. Paiva: Conceptualization, Methodology, Validation, Supervision. Pedro Paulo Balestrassi: Validation, Supervision. José Henrique G. Freitas: Validation, Investigation, Resources, Data Curation, Supervision. Vinicius C. Paes: Software, Writing - Review & Editing.

**Declaration of interests**

The authors declare that they have no known competing financial interests or personal relationships that could have appeared to influence the work reported in this paper.

The authors declare the following financial interests/personal relationships which may be considered as potential competing interests:



Simone Carneiro Streitenberger